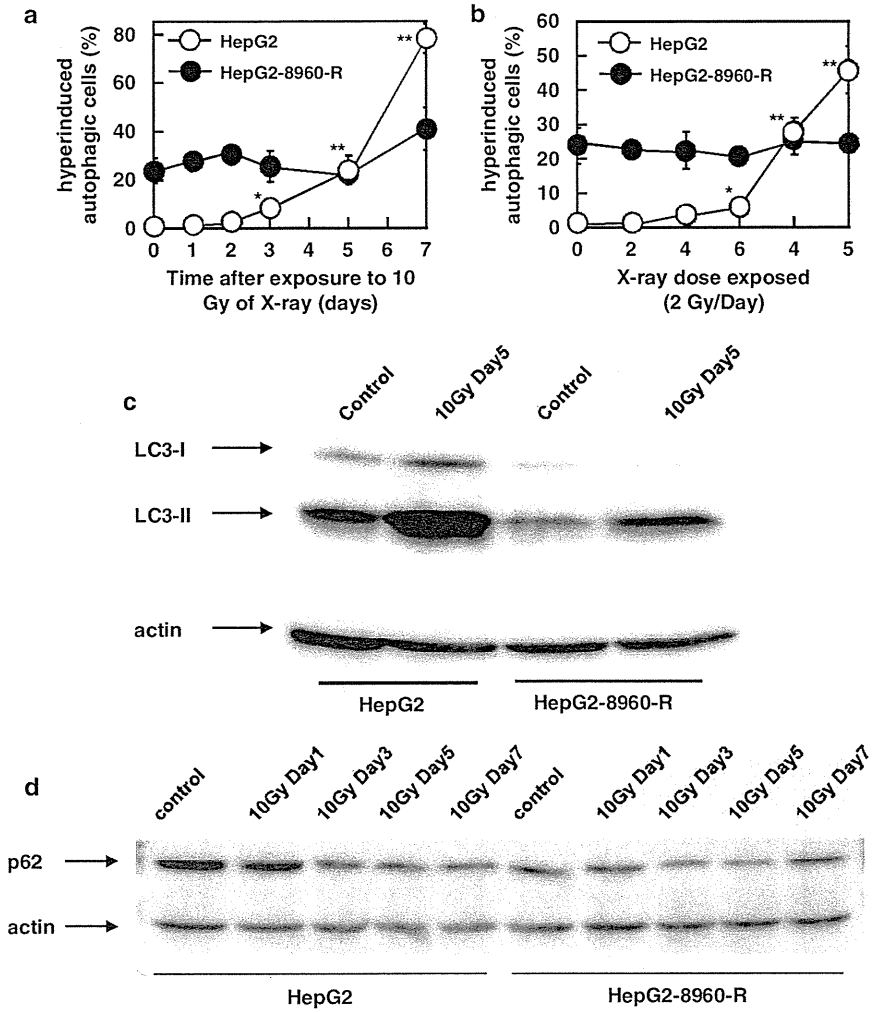

Figure 5 (**a**) Hyperinduced autophagic cells by 10 Gy of X-rays in parental HepG2 and radioresistant HepG2-8960-R cells. The induction level of hyperinduced autophagic cells in HepG2-8960-R was lower than that in HepG2. (**b**) Hyperinduced autophagic cells by fractionated 2 Gy of X-rays. Hyperinduced autophagic cells of HepG2 were gradually increased along with the dose. No increase in hyperinduced autophagic cells was observed in HepG2-8960-R after exposure to total 10 Gy of X-rays. Mean ± S.D. of three independent experiments. $^{**}P<0.01$, $^{*}P<0.05$ compared with control. (**c**) Western blot analysis of LC3 protein after X-irradiation. At day 5 after exposure to 10 Gy of X-rays, the increase in LC3-II, a hallmark of the induction of autophagy, was observed in both parental HepG2 and radioresistant HepG2-8960-R, and the amount of LC3-II in HepG2 was higher than that in HepG2-8960-R. (**d**) Western blot analysis of p62 protein after X-irradiation. At day 5 after exposure to 10 Gy of X-rays, the reduction of p62 protein, a hallmark of the induction of autophagy, was observed in both parental HepG2 and radioresistant HepG2-8960-R, and the amount of p62 protein in HepG2 was reduced much more than that in HepG2-8960-R

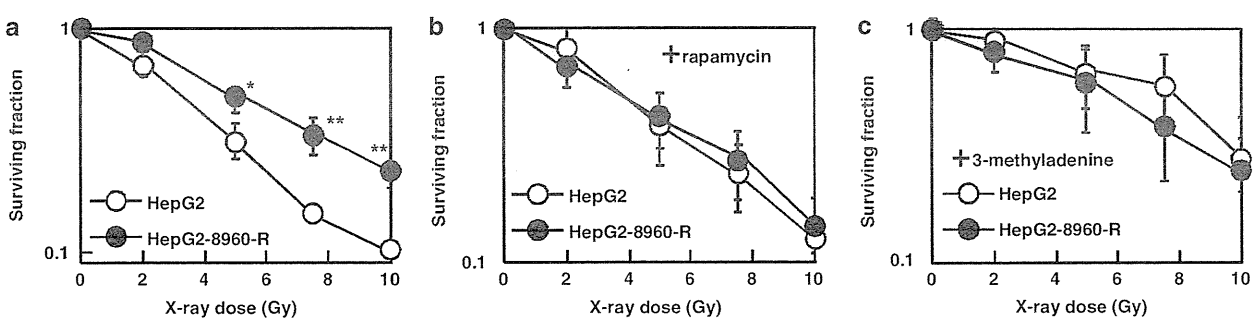

Figure 6 (**a**) HepG2-8960-R was significantly more radioresistant than HepG2 at all doses examined. (**b**) The effect of RPM on radiosensitivity of HepG2 and HepG2-8960-R. RPM canceled radioresistance of HepG2-8960-R to the levels of HepG2. (**c**) The effect of 3-MA on radiosensitivity of HepG2 and HepG2-8960-R. HepG2 cells acquired the radioresistant phenotype by the administration of 3-MA. Mean ± S.D. of three independent experiments was calculated. $^{*}P<0.05$, $^{**}P<0.01$

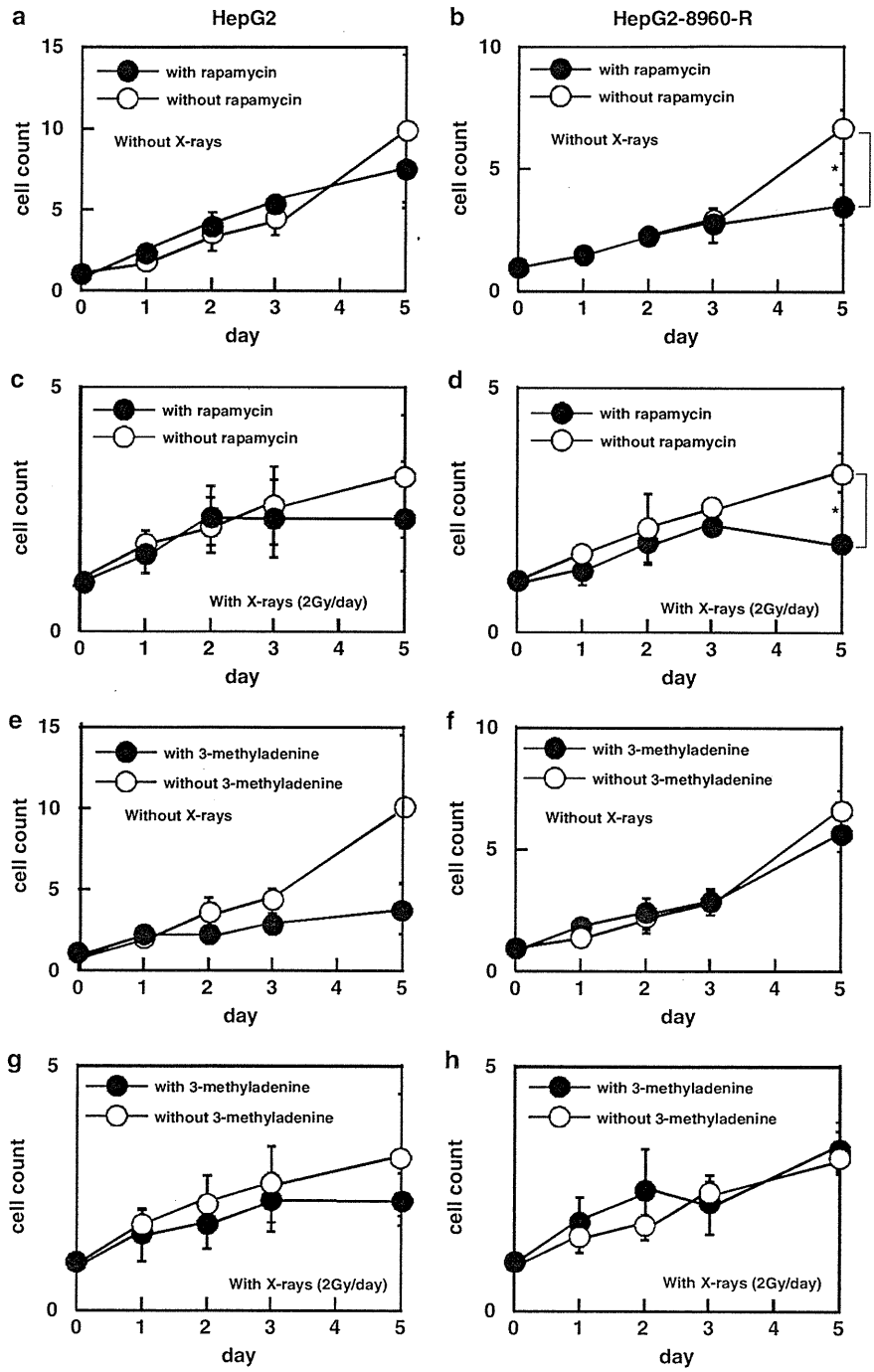

Figure 7 (**a**–**d**) Combined effect of FR of 2 Gy of X-rays (FR) and RPM on cell growth. (**a**) RPM (10 ng/ml) did not affect cell growth of HepG2. (**b**) RPM significantly suppressed cell growth of HepG2-8960-R without radiation. (**c**) Until cumulative dose of 10 Gy, RPM did not affect cell growth of HepG2. (**d**) Cell growth of HepG2-8960-R was significantly suppressed by the administration of RPM with cumulative 10 Gy of X-rays. (**e**–**h**) Combined effect of fractionated 2 Gy of X-rays and administration of 3-MA on cell growth. (**e**) Cell growth of HepG2 was suppressed by the administration of 3-MA, but no significance was detected at any point examined. (**f**) Administration of 3-MA had no effect on cell growth of HepG2-8960-R cells. (**g**) Cell growth of HepG2 with fractionated 2 Gy of X-rays was not significantly different between with and without 3-MA. (**h**) Cell growth of HepG2-8960-R with fractionated 2 Gy of X-rays was not different between with and without 3-MA. Mean ± S.D. of three independent experiments were calculated. $^{*}P<0.01$

hBeclin-1 for knockdown and siRNA-Luc for control of transfection. HepG2 gradually died out during selection for psiRNA-hBeclin-1 transfectant for three independent experiments. Without irradiation, autophagosomes were not observed both in siRNA-Luc SAS and psiRNA-hBeclin-1 SAS (Figure 8a). Five days after exposure to 10-Gy AR,

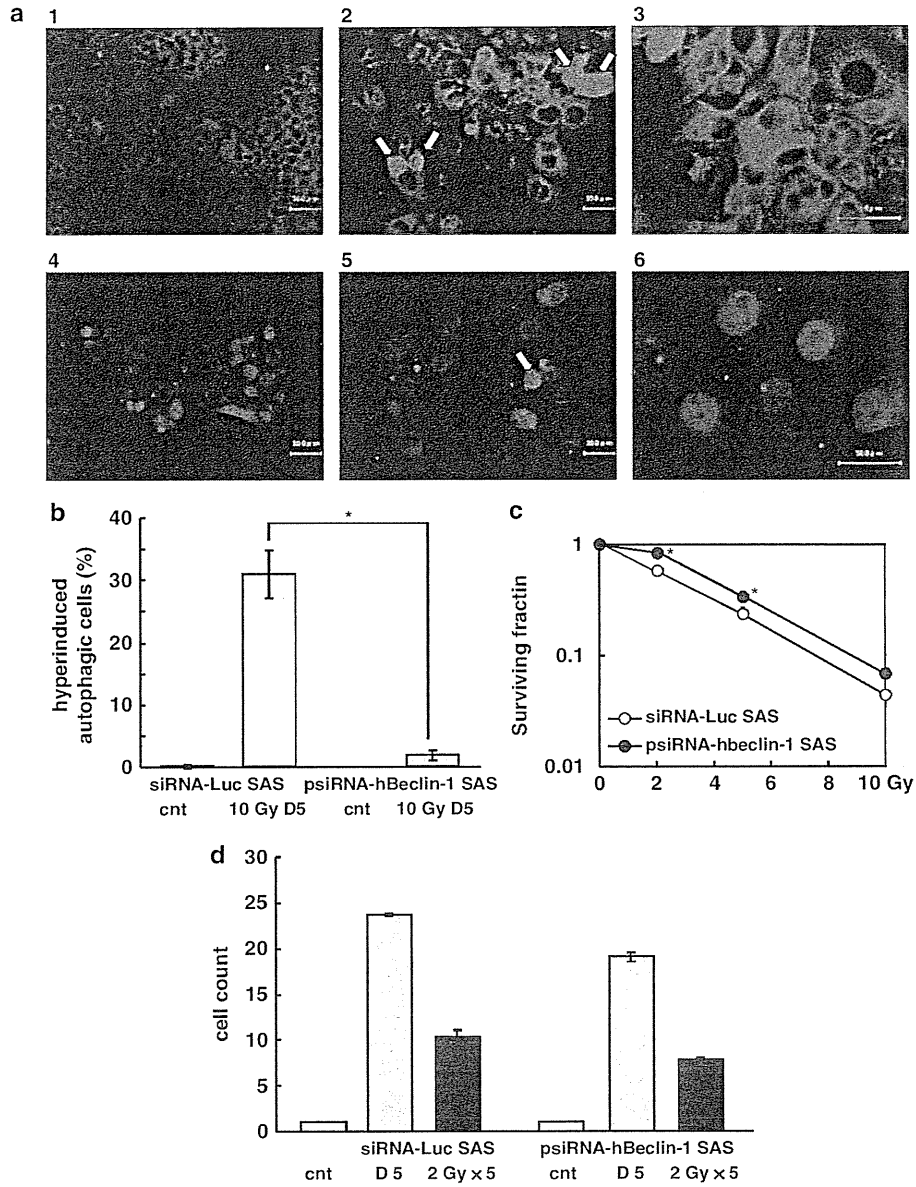

Figure 8 (a) Representative figures of autophagic cells induced by a single dose of 10-Gy X-rays in siRNA-Luc SAS and psiRNA-hBeclin-1 SAS cells. Autophagosomes were immunocytochemically visualized by anti-LC-3 antibody. (a-1) siRNA-Luc SAS cells without irradiation. (a-2) siRNA-Luc SAS cells 5 days after exposure to 10 Gy. In almost all cells the number of autophagosomes were increased. Some cells entered into hyperinduced autophagic cells (arrows). (a-3) siRNA-Luc SAS cells 5 days after exposure to 10 Gy of X-rays. High magnification. (a-4) psiRNA-hBeclin-1 SAS cells without irradiation. These cells express GFP as a marker for transfection. Therefore faint fluorescence was observed in nuclei. (a-5) psiRNA-hBeclin-1 SAS cells 5 days after exposure to 10 Gy of X-rays. Although autophagosomes were observed in cytoplasm, the number was apparently lower than that of siRNA-Luc SAS cells, indicating that induction of autophagy is suppressed by Beclin-1 knockdown. (a-6) psiRNA-hBeclin-1 SAS cells 5 days after exposure to 10 Gy of X-rays. High magnification. (b) Hyperinduced autophagic cells 5 days after exposure to 10 Gy of X-rays in siRNA-Luc SAS and psiRNA-hBeclin-1 SAS cells. (c) Radiation sensitivity of siRNA-Luc SAS and psiRNA-hBeclin-1 SAS. (d) Cell growth of siRNA-Luc SAS and psiRNA-hBeclin-1 SAS without radiation or 5×2 Gy of X-rays. Mean ± S.D. of three independent experiments. $^*P < 0.05$

increases of the nuclear size and autophagosomes were observed in siRNA-Luc SAS. On the other hand, notable increase in autophagosomes was not observed in psiRNA-hBeclin-1 SAS. These results indicated that induction of autophagy by AR is suppressed in psiRNA-hBeclin-1 SAS. Compared with siRNA-Luc SAS, induction of hyperinduced autophagic cells 5 days after exposure to AR was significantly suppressed in psiRNA-hBeclin-1 SAS (Figure 8b). We next examined whether inhibition of autophagy induces cellular radioresistance or not. Compared with siRNA-Luc SAS radioresistance of psiRNA-hBeclin-1 SAS was observed (Figure 8c). Growth rate of psiRNA-hBeclin-1 SAS was slightly slower than that of siRNA-Luc SAS (Figure 8d). Compared with un-irradiated

cells, FR of 5 × 2-Gy suppressed cell growth of both siRNA-Luc SAS and psiRNA-hBeclin-1 SAS but the suppression level was not significantly different. These results indicated that autophagy is a determinant factor of cellular radiosensitivity at least after AR of X-rays.

Discussion

Although radiotherapy is a well-established modality for various cancers, appearance of radioresistant cells is one of the major concerns. In order to understand and conquer radioresistant tumors, we have established CRR cell lines.[20,21] Profile of radiation-induced cell death under a microscope could be divided into two major types: cell death with apoptotic bodies and that lacking apoptotic bodies. We speculated that the latter was autophagic cell death. This study revealed that apoptotic changes were observed but the induction level of apoptosis was very low both in parental and CRR cells. Moreover, the inhibition of apoptosis by a caspase inhibitor, Z-VAD-FMK, did not always radiosensitize both CRR and their parental cells. These suggest that contribution of apoptosis to cellular radiosensitivity is not remarkable. One of the hallmarks of cancer cells is thought to evade apoptosis.[24,25] However, apoptosis has little or no effect on clonogenic survival after treatment with anticancer drugs or radiation in several tumor cell lines.[2] Recently, mounting evidences suggest that cancer cells can commit to death by various non-apoptotic pathways such as autophagy,[26] mitotic catastrophe and accelerated senescence.[4] In this study, maximum level of mitotic catastrophe within a week after AR was approximately 10% of HepG2 cells. This observation prompted us to examine the contribution of autophagic cell death to cellular radiosensitivity.

Autophagic cell death known as type II programmed cell death is independent of phagocytes and differs from apoptosis by the presence of autophagosomes, autolysosomes and an intact nucleus in the cell.[27] In this study, electron microscopic study revealed that radiation exposure-induced characteristic morphology to autophagic cell death. Recently, autophagy is widely investigated in the field of radiation oncology.[28] However, the role of autophagy for cellular radiosensitivity remains to be elucidated. In this study, induction of autophagy by radiation was time dependent, which is consistent with Paglin *et al.*[15] But they reported that the induction of autophagy protects cells from radiation. In this study, microscopic observation of LC3 immunocytochemistry revealed cells characterized by their cytoplasm filled with autophagosomes other than cells with a few autophagosomes. As the frequency of this distinctive type of cells increased after AR, we coined them 'hyperinduced autophagic cells'. The frequency of hyperinduced autophagic cells in parental cells increased after AR and was significantly higher than in CRR cells 7 days after AR. Western blot analysis of LC3-II revealed that the number of autophagosomes both at the basal level and the induced level after AR were lower in CRR cells than in parental cells. Western blotting of p62 revealed that the autophagy function at the basal level was higher in CRR cells than in parental cells. Both the number and the function of autophagosomes were increased by AR in parental cells while not obvious in CRR cells. These suggest that hyperinduced autophagy is associated with radiation-induced cell death albeit basal level of autophagy may contribute to the protection of cells.

RPM induces autophagy and combination with radiation facilitates the development of autophagy in human mammary carcinoma MCF-7 cells accompanied with reduction of cell survival.[29] In this study, radiosensitizing effect of RPM on parental cells was not observed, presumably because we used RPM at the concentration of 1/10 of the usually reported to avoid its toxic effects. We confirmed that this dose was enough to induce autophagy after exposure to 10 Gy in CRR cells. The HDS assay with RPM showed that lower dose of RPM than usual was enough to reverse radioresistance of CRR cells to the levels of their corresponding parental cells. Therefore, treatments with low dose RPM would be useful to sensitize radioresistant tumors. Inhibition of autophagy by 3-MA did not change radiosensitivity of CRR cells, but increased radioresistance in parental cells to the levels of corresponding CRR cells after exposure to AR. Inhibition of autophagy by knockdown of *Beclin-1* in SAS cells also induced radioresistance against AR. Lin *et al.*[30] reported that the inhibition of autophagy promotes resistance of papillary thyroid cancer (PTC) to radiation and the activation of autophagy may be a useful adjunct treatment for patients with PTC that is refractory to conventional therapy. In this study, 3-MA did not make parental cells radioresistant to FR. The frequency of hyperinduced autophagic cells in HepG2 was 80% at day 7 after exposure to 10 Gy of AR whereas 45% after exposure to 5 × 2 Gy of FR. Compared with AR the lower levels of induced autophagy by FR may partly contribute to the reason why the inhibition of autophagy either by 3-MA or Beclin-1 knockdown had lower impact on the cellular radioresistance of parental cells. In this study, we failed in obtaining Beclin-1 knockdown HepG2. This suggests that the basal level of autophagy is inevitable for cell survival though the level required is cell line dependent. Basal level of autophagy is necessary for cell survival against cellular stresses.[31] In this study, the function of autophagy at the basal level for cell protection is suggested to be higher in CRR cells than in parental cells. Radioresistance can be acquired through moderate dose of FR for 1 month.[20] These suggest that factor(s) to determine whether autophagy is involved in cell survival or cell death is different between CRR cells and parental cells.

This study also strongly suggested that the activation of autophagy may overcome tumor radioresistance. Those are consistent with reports that the activation of autophagy may yield significant benefit for cancer patients undergoing radiotherapy.[32–34] Radioresistant tumors could be surmountable by radiotherapy in combination with autophagy inducers such as RPM and RAD001 (everolimus).[35]

Radiation-induced cell death in HepG2 began to increase 4 days after AR with the increase in mitotic catastrophe. Mitotic catastrophe is a well-established response to ionizing radiation.[36] Mitotic catastrophe occurs either during or shortly after a dysregulated/failed mitosis and is thought to be the process to cell death.[37] In this study, mitotic figures started increasing 3 days after AR, suggesting that cells failed to progress mitosis go into cell death. We presented here that about 80% of HepG2 cells after exposure to AR underwent

autophagic cell death. Roughly 1/3 of cells in mitotic catastrophe were filled with autophagosomes, suggesting that these cells would die through autophagic cell death. Therefore, we think the majority of radiation-induced cell death is autophagic cell death.

This study revealed that induction of autophagy sensitized CRR cells both to AR and FR. Therefore, we conclude that the modality to induce autophagy can be one of the effective approaches to conquer radioresistant tumors.[38] We started experiments on xenografted tumors of CRR cells into nude mice to evaluate whether the inhibition of mTOR pathway is effective to eradicate radioresistant tumors or not.

Materials and Methods

Cell culture and chemicals. HepG2 cells derived from human liver cancer and SAS cells from human oral cancer were obtained from the Cell Resource Center for Biomedical Research, Institute of Development, Aging and Cancer, Tohoku University. We established CRR cell lines, HepG2-8960-R and HepG2-R from HepG2, and SAS-R from SAS independently. For the maintenance of the CRR phenotype, FR of X-rays at 2 Gy was performed every 24 h. All cells used in this study were maintained in Roswell Park Memorial Institute (RPMI) 1640 medium (Nacalai Tesque Inc., Kyoto, Japan) supplemented with 5% fetal bovine serum (Gibco Invitrogen Corp., Carlsbad, CA, USA) in a humidified atmosphere at 37 °C with 5% CO_2 in an air. In this study, acute exposure experiments were performed with cells in the exponentially growing phase and 24 h after the last maintenance irradiation.

As an inhibitor of apoptosis, Z-VAD-FMK (20 μM) was used (Promega KK, Tokyo, Japan). For the induction of autophagy, RPM (Nacalai Tesque Inc.) dissolved in ethanol (1 mg/ml) was used at the final concentration of 10 ng/ml.[39] As an inhibitor of autophagy, 3-MA (Sigma-Aldrich Inc., St. Louis, MO, USA) was used at the concentration of 1 mM by directly dissolved in culture medium before use.[40] These agents were administered in cell culture 24 h before experiments.

Irradiation. X-ray irradiation was performed in a 150-KVp X-ray generator (Model MBR-1520R, Hitachi, Tokyo, Japan) with a total filtration of 0.5 mm aluminum plus 0.1 mm copper filter at a dose rate of 1.0 Gy/min. In this study, we performed two different modes of irradiation, FR and AR. Exposure schedule of FR consisted of 2 Gy of X-rays every 24 h up to 5 days (total 10 Gy) and AR consisted of exposure to a single dose of 10-Gy X-rays.

Detection of apoptotic cells. To determine the percentage of cells undergoing apoptosis, FITC annexin V/Dead Cell Apoptosis Kit (Molecular Probes, Eugene, OR, USA) was used according to the manufacture's protocol. Briefly, after exposure to X-rays, cells were washed with PBS and stained with annexin V. Immediately after staining, annexin V-positive cells were scored under a fluorescent microscope.

Detection of mitotic catastrophe. After exposure to X-rays, cells were fixed with methyl alcohol and stained with giemsa solution. Cells with more than two nucleus and micronuclei were considered as mitotic catastrophe.

Immunocytochemical detection of autophagy. Cells were seeded on a cover slip 48 h before radiation exposure experiments. At an appropriate time after irradiation, cells were rinsed twice with phosphate-buffered saline (PBS) and then fixed with 4% paraformaldehyde in PBS for 10 min at room temperature (RT). Cells were washed twice more with PBS and immersed in 100 μg/ml of Digitonin (Wako Pure Chemical Industries, Ltd., Osaka, Japan) in PBS for 15 min at RT. After two more washings with PBS, anti-LC3 primary antibody (Medical and Biological Laboratories Co., Ltd., Nagoya, Japan) was applied. After 1-h incubation at RT, cells were washed three times with PBS (5 min each). Cells were then incubated with fluorescein-conjugated second antibody (Santa Cruz Biotechnology, Inc., Santa Cruz, CA, USA) in PBS for 30 min at RT. Then, cells were washed three times with PBS (5 min each) and Vectorshield (Vector Laboratories, Inc., Burlingame, CA, USA) was mounted onto the cover slips. Autophagosomes were visualized in a fluorescence microscope (BZ-8000, Keyence, Osaka, Japan).

The HDS assay. Cell survival was determined by the modified HDS assay.[21] Briefly, exponentially growing cells were seeded in 25 cm^2 flasks at 1×10^5 per flask for parental cells and 2.5×10^5 per flask for CRR cells. After 24-h incubation, cells were exposed to various doses of X-rays and incubated for another 72 h. Subsequently, 1/10 of the cells of each flask were seeded into another 25 cm^2 flask and incubated for further 72 h. Then total number of cells in each flask was counted by Trypan blue dye exclusion test and cell survival was plotted.

Western blot analysis. To prepare whole cell lysate, cells were washed twice with ice-cold PBS and resuspended in a lysis buffer containing 25 mM sodium phosphate (pH7.4), 500 mM NaCl, 1 mM ethylenediaminetetraacetic acid (pH 8.0), 0.5% Triton-X100, 0.1% glycerol, 5 mM $MgCl_2$, 1 mM dithiothreitol, 1 mM phenylmethylsulfonyl fluoride and Protease Inhibitor Cocktail (Nacalai Tesque Inc.). Cells were centrifuged for 20 min at 4 °C and clarified supernatants were stored at −80 °C until use. The whole cell lysate (20 μg) was electrophoresed in sodium dodecyl sulfate polyacrylamide gel and was electroblotted onto a polyvinylidene fluoride membrane. After blocking with 5% skim milk for overnight at 4 °C, the membrane was incubated for overnight with primary antibodies at 4 °C and then incubated with horseradish peroxidase-conjugated secondary antibodies (Nichirei Corporation, Tokyo, Japan). Anti-cleaved caspase-3 antibody and anti-LC3 antibody were purchased from Cell Signaling Technology Japan, KK (Tokyo, Japan) and anti-p62/SQSTM1 antibody from MBL Co., Ltd., Nagaya, Japan). Bands were visualized with Chemi-Lumi One L western blotting substrate (Nacalai Tesque Inc.).

DNA fragmentation assay. After harvesting cells including detached cells were washed twice with ice-cold PBS and genomic DNA was extracted using DNeasy Blood and Tissue Kit (Qiagen K K, Tokyo, Japan).

Cell survival after exposure to fractionated 2 Gy of X-rays. Cells (1×10^5) were seeded into a 25-cm^2 flask (Nalge Nunc International, Rochester, NY, USA) 48 h before the first experimental irradiation, and 24 h later RPM or 3-MA was administered. These cells were daily exposed to 2 Gy of X-rays for 5 consecutive days without medium exchange. At the appropriate time point during this experiment, total number of cells was scored and relative value of control was calculated.

Electron microscopy. HepG2 cells grown in 60-mm culture dishes were washed twice with PBS. Cells were fixed in 100 mM phosphate buffer, pH 7.4, containing 2.5% glutaraldehyde for 30 min at 4 °C. The cells were rinsed twice with ice-cold PBS, post-fixed in OsO_4, dehydrated in graded acetone and embedded in epoxy resin. Ultrathin sections were prepared with Ultra-microtome (Leica Microsystems Japan, Tokyo, Japan), mounted in copper grids, and counterstained with uranyl acetate and lead citrate. Photographs were obtained using transmission electron microscope (Hitachi High-Technologies Corporation, Tokyo, Japan).

Inhibition of autophagy by Beclin-1 knockdown. In order to inhibit autophagy, a psiRNA-hBeclin-1 Kit was used according to the manufacture's protocol (*Invivo*Gen, San Diego, CA, USA). Briefly, cells were transfected with expression vector using HilyMax (Dojindo, Kumamoto, Japan). These cells were cultured in RPMI medium containing 5% fetal bovine serum and Zeocin (100 μg/ml, *Invivo*Gen) for 2 weeks. The viable cell preparation was used for experiments.

Statistical analysis. At each data point, the mean and S.D. were calculated and statistically analyzed using Student's *t*-test.

Conflict of Interest

The authors declare no conflict of interest.

Acknowledgements. We thank Biomedical Research Core of Tohoku University Graduate School of Medicine for technical support. This study was in part supported by the Grant-in-Aid for young scientists from Ministry of Education, Culture, Sports, Science and Technology, by a grant from RADIATION EFFECT ASSOCIATION and by a grant from the Ministry of Health, Labour and Welfare of Japan.

1. Schmitt CA, Fridman JS, Yang M, Lee S, Baranov E, Hoffman RM *et al.* A senescence program controlled by p53 and p16INK4a contributes to the outcome of cancer therapy. *Cell* 2002; **109**: 335–346.
2. Roninson IB, Broude EV, Chang BD. If not apoptosis, then what? Treatment-induced senescence and mitotic catastrophe in tumor cells. *Drug Resist Updat* 2001; **4**: 303–313.
3. Kondo Y, Kanzawa T, Sawaya R, Kondo S. The role of autophagy in cancer development and response to therapy. *Nat Rev Cancer* 2005; **5**: 726–734.
4. Gewirtz DA, Holt SE, Grant S. *Apoptosis, Senescence and Cancer*, 2nd edn. Humana Press: Totowa, NJ, USA, 2007.
5. Endlich B, Radford IR, Forrester HB, Dewey WC. Computerized video time-lapse microscopy studies of ionizing radiation-induced rapid-interphase and mitosis-related apoptosis in lymphoid cells. *Radiat Res* 2000; **153**: 36–48.
6. Kim R, Emi M, Tanabe K, Uchida Y, Arihiro K. The role of apoptotic or nonapoptotic cell death in determining cellular response to anticancer treatment. *Eur J Surg Oncol* 2006; **32**: 269–277.
7. Finkel E. Does cancer therapy trigger cell suicide? *Science* 1999; **286**: 2256–2258.
8. Brown JM, Wouters BG. Apoptosis, p53, and tumor cell sensitivity to anticancer agents. *Cancer Res* 1999; **59**: 1391–1399.
9. Brown JM, Wilson G. Apoptosis genes and resistance to cancer therapy: what does the experimental and clinical data tell us? *Cancer Biol Ther* 2003; **2**: 477–490.
10. Ogier-Denis E, Codogno P. Autophagy: a barrier or an adaptive response to cancer. *Biochim Biophys Acta* 2003; **1603**: 113–128.
11. Gozuacik D, Kimchi A. Autophagy as a cell death and tumor suppressor mechanism. *Oncogene* 2004; **23**: 2891–2906.
12. Cuervo AM. Autophagy: in sickness and in health. *Trends Cell Biol* 2004; **14**: 70–77.
13. Bursch W, Ellinger A, Kienzl H, Torok L, Pandey S, Sikorska M *et al.* Active cell death induced by the anti-estrogens tamoxifen and ICI 164 384 in human mammary carcinoma cells (MCF-7) in culture: the role of autophagy. *Carcinogenesis* 1996; **17**: 1595–1607.
14. Bauvy C, Gane P, Arico S, Codogno P, Ogier-Denis E. Autophagy delays sulindac sulfide-induced apoptosis in the human intestinal colon cancer cell line HT-29. *Exp Cell Res* 2001; **268**: 139–149.
15. Paglin S, Hollister T, Delohery T, Hackett N, McMahill M, Sphicas E *et al.* A novel response of cancer cells to radiation involves autophagy and formation of acidic vesicles. *Cancer Res* 2001; **61**: 439–444.
16. Jia L, Dourmashkin RR, Allen PD, Gray AB, Newland AC, Kelsey SM. Inhibition of autophagy abrogates tumour necrosis factor alpha induced apoptosis in human T-lymphoblastic leukaemic cells. *Br J Haematol* 1997; **98**: 673–685.
17. Shintani T, Klionsky DJ. Autophagy in health and disease: a double-edged sword. *Science* 2004; **306**: 990–995.
18. Yao KC, Komata T, Kondo Y, Kanzawa T, Kondo S, Germano IM. Molecular response of human glioblastoma multiforme cells to ionizing radiation: cell cycle arrest, modulation of the expression of cyclin-dependent kinase inhibitors, and autophagy. *J Neurosurg* 2003; **98**: 378–384.
19. Apel A, Zentgraf H, Buchler MW, Herr I. Autophagy-A double-edged sword in oncology. *Int J Cancer* 2009; **125**: 991–995.
20. Kuwahara Y, Li L, Baba T, Nakagawa H, Shimura T, Yamamoto Y *et al.* Clinically relevant radioresistant cells efficiently repair DNA double-strand breaks induced by X-rays. *Cancer Sci* 2009; **100**: 747–752.
21. Kuwahara Y, Mori M, Oikawa T, Shimura T, Ohtake Y, Mori S *et al.* The modified high-density survival assay is the useful tool to predict the effectiveness of fractionated radiation exposure. *J Radiat Res* 2010; **51**: 297–302.
22. Kabeya Y, Mizushima N, Ueno T, Yamamoto A, Kirisako T, Noda T *et al.* LC3, a mammalian homologue of yeast Apg8p, is localized in autophagosome membranes after processing. *EMBO J* 2000; **19**: 5720–5728.
23. Bjorkoy G, Lamark T, Pankiv S, Overvatn A, Brech A, Johansen T. Monitoring autophagic degradation of p62/SQSTM1. *Methods Enzymol* 2009; **452**: 181–197.
24. Hanahan D, Weinberg RA. The hallmarks of cancer. *Cell* 2000; **100**: 57–70.
25. Lefranc F, Facchini V, Kiss R. Proautophagic drugs: a novel means to combat apoptosis-resistant cancers, with a special emphasis on glioblastomas. *Oncologist* 2007; **12**: 1395–1403.
26. Fujiwara K, Iwado E, Mills GB, Sawaya R, Kondo S, Kondo Y. Akt inhibitor shows anticancer and radiosensitizing effects in malignant glioma cells by inducing autophagy. *Int J Oncol* 2007; **31**: 753–760.
27. Reggiori F, Klionsky DJ. Autophagosomes: biogenesis from scratch? *Curr Opin Cell Biol* 2005; **17**: 415–422.
28. Zois CE, Koukourakis MI. Radiation-induced autophagy in normal and cancer cells: towards novel cytoprotection and radio-sensitization policies? *Autophagy* 2009; **5**: 442–450.
29. Paglin S, Lee NY, Nakar C, Fitzgerald M, Plotkin J, Deuel B *et al.* Rapamycin-sensitive pathway regulates mitochondrial membrane potential, autophagy, and survival in irradiated MCF-7 cells. *Cancer Res* 2005; **65**: 11061–11070.
30. Lin CI, Whang EE, Abramson MA, Jiang X, Price BD, Donner DB *et al.* Autophagy: a new target for advanced papillary thyroid cancer therapy. *Surgery* 2009; **146**: 1208–1214.
31. Mizushima N, Levine B, Cuervo AM, Klionsky DJ. Autophagy fights disease through cellular self-digestion. *Nature* 2008; **451**: 1069–1075.
32. Dalby KN, Tekedereli I, Lopez-Berestein G, Ozpolat B. Targeting the prodeath and prosurvival functions of autophagy as novel therapeutic strategies in cancer. *Autophagy* 2010; **6**: 322–329.
33. Turcotte S, Giaccia AJ. Targeting cancer cells through autophagy for anticancer therapy. *Curr Opin Cell Biol* 2010; **22**: 246–251.
34. Moretti L, Yang ES, Kim KW, Lu B. Autophagy signaling in cancer and its potential as novel target to improve anticancer therapy. *Drug Resist Updat* 2007; **10**: 135–143.
35. Lin CI, Whang EE, Donner DB, Du J, Lorch J, He F *et al.* Autophagy induction with RAD001 enhances chemosensitivity and radiosensitivity through Met inhibition in papillary thyroid cancer. *Mol Cancer Res* 2010; **8**: 1217–1226.
36. Vakifahmetoglu H, Olsson M, Zhivotovsky B. Death through a tragedy: mitotic catastrophe. *Cell Death Differ* 2008; **15**: 1153–1162.
37. Kroemer G, Galluzzi L, Vandenabeele P, Abrams J, Alnemri ES, Baehrecke EH *et al.* Classification of cell death: recommendations of the Nomenclature Committee on Cell Death 2009. *Cell Death Differ* 2009; **16**: 3–11.
38. Ciuffreda L, Di Sanza C, Incani UC, Milella M. The mTOR pathway: a new target in cancer therapy. *Curr Cancer Drug Targets* 2010; **10**: 484–495.
39. Rubinsztein DC, Gestwicki JE, Murphy LO, Klionsky DJ. Potential therapeutic applications of autophagy. *Nat Rev Drug Discov* 2007; **6**: 304–312.
40. Kanzawa T, Germano IM, Komata T, Ito H, Kondo Y, Kondo S. Role of autophagy in temozolomide-induced cytotoxicity for malignant glioma cells. *Cell Death Differ* 2004; **11**: 448–457.

Supplementary Information accompanies the paper on Cell Death and Disease website (http://www.nature.com/cddis)

Leukemia Research 35 (2011) 1484–1490

Contents lists available at ScienceDirect

Leukemia Research

journal homepage: www.elsevier.com/locate/leukres

Involvement of osteopontin and its signaling molecule CD44 in clinicopathological features of adult T cell leukemia

Haorile Chagan-Yasutan[a], Kunihiro Tsukasaki[b], Yayoi Takahashi[c], Shigeru Oguma[d], Hideo Harigae[e], Naoto Ishii[f], Jing Zhang[g], Manabu Fukumoto[h], Toshio Hattori[a,*]

[a] Division of Emerging Infectious Diseases, Department of Internal Medicine, Graduate School of Medicine, Tohoku University, 2-1 Seiryo-cho, Aoba-ku, Sendai 980-8574, Japan
[b] Department of Molecular Medicine and Hematology, Molecular Medicine Unit, Atomic Bomb Disease Institute, Nagasaki University Graduate School of Biomedical Science, Nagasaki, Japan
[c] Department of Pathology, Tohoku University Hospital, Sendai, Japan
[d] Medical Informatics Division, Takeda General Hospital, Kyoto, Japan
[e] Division of Hematology and Rheumatology, Tohoku University Hospital, Sendai, Japan
[f] Division of Microbiology and Immunology, Graduate School of Medicine, Tohoku University, Sendai, Japan
[g] Research and Development Center, FUSO Pharmaceutical Industries, Ltd, Osaka, Japan
[h] Division of Cancer Control Pathology, Institute of Development, Aging and Cancer, Tohoku University, Sendai, Japan

ARTICLE INFO

Article history:
Received 30 March 2011
Received in revised form 6 May 2011
Accepted 9 May 2011
Available online 6 June 2011

Keywords:
ATL
OPN
CD44
CD44v6
Prognostic factors
Immunohistochemical staining

ABSTRACT

We previously reported that the osteopontin (OPN) gene as well as CD44 is trans-activated by the Tax protein of HTLV-1, however the synthesis of both in adult T cell leukemia (ATL) has not been described yet. Here we showed the expression of these molecules in plasma and tissue of ATL. Significant differences were found among the normal and four subtypes of 27 ATL patients in plasma levels of OPN ($p = 3.6 \times 10^{-6}$) and soluble CD44 ($p < 0.001$) and they were significantly related to each other ($p < 0.002$). Also they were significantly associated with the performance status, total number of involved lesions, and lactic dehydrogenase, and inversely with lymphocyte count ($p < 0.01$). Immunohistochemical staining of lymph-nodes and skin from 7 ATL patients using anti-OPN and anti-CD44 antibodies demonstrated that both expressions were weak/moderate in ATL cells but moderate/strong in infiltrated macrophages in 6 patients. These results demonstrate that OPN and CD44 play important roles in tumor formations and their products in plasma could be markers of the severity in ATL.

1. Introduction

Adult T cell leukemia (ATL) was the first human cancer found to be caused by a retrovirus, human T cell lymphotropic virus type-1 (HTLV-1) [1,2]. Its clinical entity was established in Japan [3], and the discovery of HTLV-1 enabled the molecular diagnosis of ATL, which has been classified into acute, chronic, lymphoma and smoldering types reflecting their diverse clinical features and prognosis [4]. The prognosis of acute and lymphoma-type ATL patients is extremely poor despite the introduction of intensive chemotherapy and allogeneic hematopoietic transplantation [5].

The clinical manifestation of ATL is usually characterized by leukocytosis, lymphadenopathy, hepatosplenomegaly, skin eruption, thrombocytopenia and hypercalcemia [3–5]. Most ATL cells are mature helper T cell phenotypes $CD3^+$, $CD4^+$, $CD8^-$, and $CD25^+$, with some exceptions such as double negative or double positive CD4 and CD8 [6,7]. The pathological findings of ATL cells are (1) diffuse proliferation of the neoplastic cells, (2) pleomorphism of the neoplastic cells with markedly deformed nuclei, (3) heterogeneous histological features of lymph nodes admixed with a cluster of non-malignant lymphocytes, proliferation of macrophages and well developed high endothelium venules and (4) high incidence of skin lesions due to the infiltration of neoplastic cells [8].

HTLV-1 infection is usually asymptomatic, but it can cause ATL after a long latency period. A study performed in Nagasaki, Japan showed that the lifetime risk to develop ATL among 100,000 HTLV-1 infected carriers aged 30 or older was approximately 6.6% (95% CI 3.8–9.2) for men and 2.1% (95% CI 1.0–3.1) for women [9]. Although the mechanisms of such leukemogenesis are still not clear, numerous studies have been done to clarify how cancer develops from HTLV-1. HTLV-1 does not have an oncogene, but does have a unique gene tax which activates long-terminal-repeat (LTR) in trans [10]. Accordingly, a number of reports showed that cytokines and chemokines such as IL-1, IL-13, and IL-9 are synthesized by ATL cells [11–13]. But it is also true that tax expression is very low or undetectable in primary ATL cells [14].

* Corresponding author. Tel.: +81 22 717 8220; fax: +81 22 717 8221.
E-mail address: hatori286@yahoo.co.jp (T. Hattori).

0145-2126/$ – see front matter © 2011 Elsevier Ltd. All rights reserved.
doi:10.1016/j.leukres.2011.05.011

Table 1
Clinical characteristics of ATL patients.

Characteristics	Ref. range	Median (range)			
		Acute	Lymphoma	Chronic	Smoldering
WBC ($\times 10^3/\mu l$)	3.2–9.6	34 (7.4–203)	3.2 (3–7.8)	12.9 (5.3–22.7)	6.8 (6.3–7.2)
HB (g/dL)	13–17	13.6 (11.7–17.4)	11 (10.4–12.6)	12.1 (11.5–15.8)	12.8 (11.4–14.2)
PLT ($\times 10^3/\mu l$)	131–362	173 (98–399)	172 (135–185)	249 (152–334)	215 (214–216)
Ly (%)	22–55	6 (0–18)	30 (26–45)	31 (14–58)	30.5 (29–32)
Abnormal Ly (%)	0	51 (6–96)	1 (0–1)	11 (5–70)	19.5 (7–32)
CRP (mg/dL)	0–0.3	0.9 (0.23–3.8)	0.9 (0.23–1.5)	0.2 (0.05–3)	0.1 (0.03–0.1)
PS-0/1/2, 3/4	0	2 (1–4)	1 (1–1)	1 (0–1)	0 (0–0)
TIL-1/2–3/≥4, 5	0	4 (2–5)	2 (1–2)	1 (1–3)	1 (1–1)
LDH (U/L)	119–229	1075 (150–9165)	502 (203–639)	217 (155–361)	193 (187–199)
sIL2R (U/ml)	145–519	108,084 (1902–127,703)	8084 (2266–61,388)	1530 (798–12,575)	1412 (543–2280)
Hypercalcemia (Y/N)	N	8Y/5N	N	N	N
OPN (ng/ml)	<396	843 (438–2965)	800 (471–1023)	318 (122–716)	259 (196–321)
sCD44 (ng/ml)	<194	441 (68–897)	257 (135–524)	125 (94–395)	193 (174–212)

Abbreviations: ATL, adult T cell Leukemia; WBC, white blood cell; HB, hemoglobin; PLT, platelet counts; Ly, lymphocyte; CRP, C-reactive protein; PS, performance status; TIL, total involved lesions; LDH, lactic dehydrogenase; sIL-2R, soluble interleukin 2 receptor; OPN, osteopontin; sCD44, soluble CD44; Y, yes; N, no.

OPN is a secreted glycoprotein that interacts both with CD44 and integrin including α4β1, α4β7, α9β1 [15,16]. OPN promotes the migration and invasion of tumor cells, inhibits apoptosis, and facilitates extracellular matrix remolding and angiogenesis by interacting with its receptors on various types of cells [17]. OPN is widely distributed in the body and secreted by a wide range of cells such as macrophages, activated T cells, endothelial cells, and vascular muscle cells [15]. It is also a pro-inflammatory marker in various infectious diseases [18]. In a recent study, circulating OPN was described as the only cytokine elevated in mice bearing instigating tumors as opposed to non-instigating tumors [19]. CD44 is a broadly distributed transmembrane glycoprotein originally identified as a receptor for hyaluronan [20], and OPN was also proposed to be a ligand for CD44 [21]. It is synthesized in multiple isoforms that consists of the smallest CD44, which is known as standard CD44, and several larger variant isoforms, CD44v1-10 [22]. In clinical studies of patients with cancer, enhanced CD44 of the standard form as well as its variants forms, especially CD44v6, was correlated with poor prognosis [23,24]. We have reported that the OPN gene as well as CD44 is trans-activated by the Tax protein of HTLV-1 via PI3 K/AKT and noncanonical nuclear factor (NF-κB) signaling pathway, respectively [25,26]. However, the synthesis of both OPN and CD44 in ATL patients has not been described yet. Therefore, we measured the levels of OPN and soluble CD44 (sCD44) in the plasma of ATL patients to explore their relationship with various clinical prognostic factors. In addition, we examined whether these molecules are expressed in ATL cells in the involved lymph nodes and skin of patients using immunohistochemical staining and also in ATL cell line in vitro by FACS, and discussed the clinicopathological roles of these molecules in ATL.

2. Materials and methods

2.1. Plasma

We collected heparin plasma samples of 27 ATL patients from Nagasaki University Hospital, in which 13 were acute, 3 were lymphoma, 9 were chronic and 2 were the smoldering subtypes. The mean age and sex in each subtype were as follows: acute, 60 ± 13.6 years old (yr), 10 males (M)/3 females (F); lymphoma, 65 ± 14.5 yr, 2 M/1F; chronic, 56 ± 16.2 yr, 4M/5F; smoldering, 66 ± 6.4 yr, 1M/1F. These patients were clinically diagnosed as ATL based on the accepted criteria for clinical, hematological and laboratory findings during the years 1991–2006. Samples were collected before treatment. Plasma was obtained by centrifugation at 3000 rpm for 10 min at 4 °C and was aliquoted to cryotubes and stored at −80 °C until use. Multiple thawing was avoided. All work was conducted in accordance with the Declaration of Helsinki. This study was approved by the Ethics Committees of Tohoku University Hospital (2007-257) and Nagasaki University Hospital (14090570). In addition, plasmas from 30 healthy individuals (28 ± 8 yr, 10M/20F) were included as the normal control.

2.2. Clinical data

The performance status (PS) (0/1/2, 3/4), total involved lesions (TIL) (1/2–3/≥4, 5), lactic dehydrogenase (LDH), lymphocyte (Ly) (%), white blood cell numbers (WBC), platelet count (PLT) and other laboratory markers were measured in Nagasaki University Hospital (Table 1).

2.3. Enzyme-linked immuno sorbent assay (ELISA)

OPN in the plasma and in the supernatant of the cell lines was measured using a human osteopontin Elisa kit (Immuno-Biological Laboratories, Gunma, Japan) as described previously [18,27]. Plasma sCD44 was determined by Human CD44 Elisa Kit (Abcam, Japan) [28]. All measurements were based on the average of triplicate samples. Both the OPN and sCD44 levels in plasma were expressed as ng/ml. The cut-off points to divide high and low plasma OPN and sCD44 were 396 ng/ml and 194 ng/ml, respectively based on the levels of normal control group (mean + 2SD, $n = 30$).

2.4. Histological analysis

Tissues from lymph-nodes and skin from 7 ATL patients were analyzed. This study was approved by the Tohoku University Ethics Committee (2007-413). The tissues were fixed in 10% formalin and histological specimens for pathological diagnosis and then the immunohistochemical staining were treated according to usual methods as described previously [29]. We examined the expression of OPN and its receptor CD44, and CD44v6 because CD44v6 is known to be induced in tumor cells by the interaction of OPN with its receptor, CD44 and/or integrin [30]. CD68, a marker of macrophages, was also used.

For OPN staining, antigen retrieval was performed in an autoclave (120 °C, 5 min) and anti-OPN monoclonal antibody (mAb) (1:250 dilution, MPIIIB10$_1$, DSHB) was used as the primary antibody [31] with a signal amplification staining system (CSA II, Dako). For CD68, CD44 and CD44v6 staining, antigen retrieval was done by trypsin treatment (0.05%) for 30 min at 37 °C, and anti-CD68 (1:200 dilution, clone: PG-M1, DAKO), anti-CD44 (1:2000 dilution, clone: 2C5, R&D) or anti-CD44v6 (1:250 dilution, clone: VFF-7, Abcam) mAbs were used.

The expression levels were evaluated according to the proportion and intensity of the granulation on the tumor area; the intensity of the staining was recorded as follows: –, negative; +/–, weakly positive; +, moderately positive; ++, strongly positive.

2.5. Cells

43-T and ED40515 of ATL cell lines were kindly provided by Dr. Maeda from Kyoto University, and were cultured in RPMI1640 medium supplemented with 10% heat-inactivated fetal calf serum (FCS), 50 U/ml penicillin and 50 μg/ml streptomycin. Both cell lines are known to be derived from a leukemic clone. 43-T was established from a patient with gastrointestinal involvement [32]. In addition, a macrophage cell line, A-THP-1, from Cell Resource Center for Biomedical Research Institute of Development, Aging and Cancer (Tohoku University) was used in the same condition as described above [33]. The supernatant of these cells were collected after four days culture of 1.5–2.0 × 10^6 in 10 ml of culture.

2.6. Flow cytometric analysis

43-T and ED40515 cells were first grown in FBS free RPMI medium for 24 h at 37 °C with 5% CO_2 and cultured with or without 3 μg recombinant OPN (R&D, Minneapolis) or the medium containing 10% supernatant of A-THP-1, a macrophage

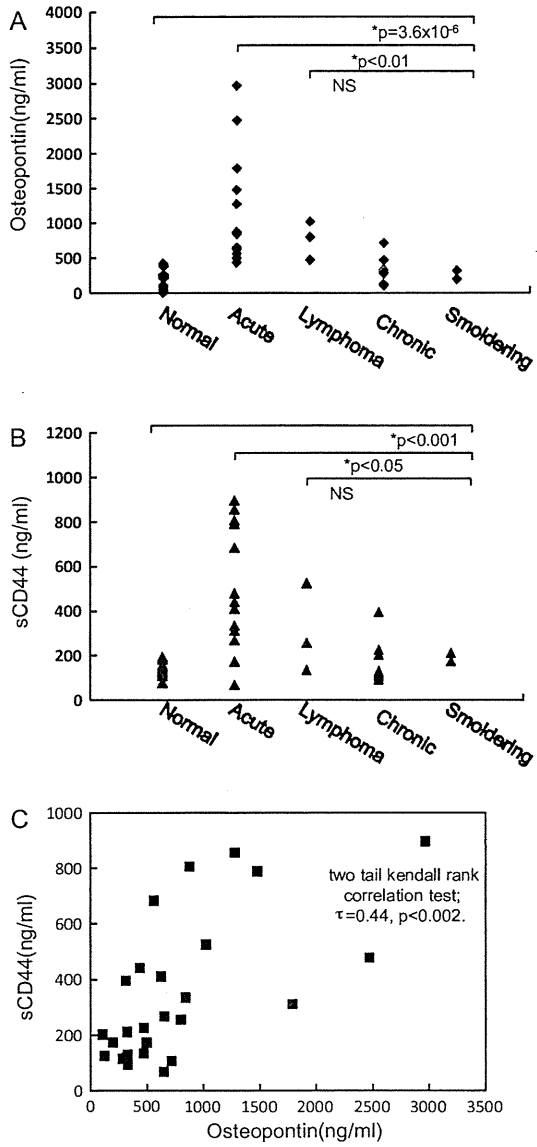

Fig. 1. The plasma levels of osteopontin and sCD44 in normal and four subtypes of ATL and their relationships. Plasma OPN and sCD44 were measured in 27 cases of ATL patients and 30 normal control individuals. (A) OPN. The median levels of the plasma OPN were apparently higher in the acute type (843 ng/ml, range 438–2965 ng/ml) compared with the lymphoma (800 ng/ml, range 471–1023 ng/ml), chronic (318 ng/ml, range 122–716 ng/ml), or smoldering (259 ng/ml, 196–321 ng/ml) types of ATL. The levels were significantly different among normal and ATL subtypes and among the four subtypes, but not among subtypes when excluding acute ATL according to the two tail Kruskal–Wallis test ($p = 3.6 \times 10^{-6}$, $p < 0.01$, not significant (NS), respectively). Following Dunn's post test analysis showed that significant differences were found between normal and acute type ATL ($p < 0.0001$), and lymphoma type ATL ($p < 0.05$). (B) sCD44. The levels of plasma sCD44 in ATL were as follows: acute type (441 ng/ml, range 68–897 ng/ml), lymphoma type (257 ng/ml, range 135–524 ng/ml), chronic type (125 ng/ml, range 94–395 ng/ml), and smoldering (193 ng/ml, range 174–212 ng/ml). The results of the statistical analyses were essentially similar to those of OPN and were significantly different among groups according to the two tail Kruskal–Wallis test ($p < 0.001$, $p < 0.05$, NS, respectively). Significant differences were found between acute type ATL and normal ($p < 0.0001$), and chronic type ATL ($p < 0.01$) by Dunn's post test. (C) The relationships between the levels of OPN and sCD44 were assessed by two tail Kendall rank correlation test and the result showed a significant correlation between them in ATL patients ($n = 27$, τ (Kendall's tau coefficient) = 0.44, $p < 0.002$).

cell line. After 30 min incubation at 4°C, cells were harvested and stained with mouse anti-human mAbs against CD44, CD44v6 (Abcam), CD49d (integrin α4), CD29 (integrin β1), integrin β7 (Biolegend), CD25 (BD Biosciences) and HLA-DR (BD Biosciences). All the mAbs were labelled with FITC or PE, and the stained cells were analyzed using a FACS Calibur Cytometer (BD Bioscience).

2.7. Statistical analysis

The Kruskal–Wallis test was used for estimating differences in the OPN and sCD44 levels among normal, acute, lymphoma, chronic and smoldering subtypes. Following the test, the two tail Dunn's post test was calculated to compare differences in each pair. Kendall rank correlation test were used for determining the relationship between the clinical data and plasma levels of OPN and sCD44.

3. Results

3.1. Elevated levels of plasma OPN and sCD44 in ATL patients

Plasma OPN and sCD44 were measured in 27 cases of ATL patients and 30 normal control individuals. The median levels of the plasma OPN were apparently higher in the acute type (843 ng/ml, range 438–2965 ng/ml) compared with lymphoma (800 ng/ml, range 471–1023 ng/ml), chronic (318 ng/ml, range 122–716 ng/ml), or smoldering (259 ng/ml, 196–321 ng/ml) types of ATL (Table 1). The levels were significantly different among normal and ATL subtypes and among the four subtypes, but not among the subtypes when excluding acute ATL according to the two tail Kruskal–Wallis test ($p = 3.6 \times 10^{-6}$, $p < 0.01$, $p = 0.1$, respectively) (Fig. 1A). Dunn's post test analysis showed that significant differences were found between normal and acute type ATL ($p < 0.0001$), and between normal and lymphoma type ATL ($p < 0.05$). It is of note that high OPN (>396 ng/ml) was found in all of the 13 acute and 3 lymphoma type patients and in 2 of the chronic type.

The levels of plasma sCD44 in ATL were also measured. The results were as follows: acute type (441 ng/ml, range 68–897 ng/ml), lymphoma type (257 ng/ml, range 135–524 ng/ml), chronic type (125 ng/ml, range 94–395 ng/ml), and smoldering (193 ng/ml, range 174–212 ng/ml) (Table 1). The results of statistical analyses were essentially similar to those of OPN and were significantly different among the groups according to the two tail Kruskal–Wallis test (Fig. 1B). Significant differences were found between acute type ATL and normal ($p < 0.0001$), and between acute and chronic type ATL ($p < 0.01$) by Dunn's post test. However, differing from the levels of OPN, the levels of sCD44 were lower than the cut-off point (194 ng/ml) in 2 acute patients and 1 lymphoma patient. Further, the relationships between the levels of OPN and sCD44 were assessed by two tail Kendall rank correlation test and the result showed a significant correlation between them in the ATL patients ($n = 27$, τ (Kendall's tau coefficient) = 0.44, $p < 0.002$) (Fig. 1C), but not in the normal individuals ($n = 30$, $p = 0.1$).

3.2. Plasma levels of OPN and sCD44 correlated with disease severity in ATL

At present, several major prognostic indicators for ATL have been described, such as advanced PS, more than three TIL, high LDH, hypercalcemia and older than 40 years [34]. The correlations between the levels of plasma OPN and sCD44 with the above clinical data were estimated by two tails Kendall rank test. The plasma OPN levels were found to have significant positive correlations with PS ($p < 0.001$), TIL ($p < 0.01$) and LDH ($p < 0.05$) and an inverse correlation with Ly ($p < 0.05$). The plasma sCD44 levels were also positively correlated with PS ($p < 0.01$), TIL ($p < 0.05$), LDH ($p < 0.001$), and with soluble interleukin-2 receptor (sIL-2R) ($p < 0.05$) and WBC ($p < 0.05$); an inverse correlation was found with PLT ($p < 0.01$) and Ly ($p < 0.001$) (Table 2).

Table 2
The relationship between clinical characteristics and plasma levels of OPN and sCD44 of ATL patients.

Characteristics	OPN (ng/ml)		sCD44 (ng/ml)	
	τ	p	τ	p
WBC ($\times 10^3$/ml)	0.13	0.32	0.28	0.04*
HB (g/dL)	0.09	0.50	−0.008	0.5
PLT ($\times 10^3$/ml)	−0.15	0.27	−0.43	0.002**
Ly (%)	−0.34	0.01*	−0.5	0.0001***
Abnormal Ly (%)	0.15	0.26	0.2	0.09
CRP (mg/dL)	0.21	0.19	0.13	0.4
PS (0/1/2, 3/4)	0.48	0.0006***	0.4	0.004**
TIL (1/2–3/≥4, 5)	0.37	0.008**	0.3	0.03*
LDH (U/L)	0.31	0.02*	0.5	0.0002***
SIL-2R (U/ml)	0.31	0.07	0.52	0.03*

Statistical analysis was made by Kendal-rank test, τ means Kendall's tau coefficient.
* $p<0.05$.
** $p<0.01$.
*** $p<0.01$.

3.3. OPN was synthesized not only by ATL cells but also by other cells

To define the synthesizing cells in tissue, we examined the expression of OPN, CD44, and CD44v6 expression using tissues from lymph nodes and skin from ATL patients. CD68 was also used because macrophage cells are known to be OPN producers. The tissues were infiltrated with diffusely proliferating tumor cells with markedly deformed nuclei, macrophages and normal lymphocytes [8].

Our immunohistochemical staining showed that the infiltrated macrophages, which were identified by anti-CD68 mAb expressed OPN moderately or strongly in all cases but the infiltration of macrophages was also variable as only a few macrophage cells were seen in patient 2 (Table 3 and Fig. 2A). Furthermore, tumor cells were also positive for OPN staining in the tissues of ATL (Table 3 and Fig. 2A); however, the staining intensities were not so strong despite the amplification. The cells of epidermis abundantly expressed OPN and some of the infiltrated ATL cells also expressed OPN (patient 2) (Fig. 2A). It is possible that OPN synthesized by epidermal cells attract ATL cells to skin. In nasal cavity-associated lymphoid tissue (NALT) (patient 3), OPN was expressed by macrophage cells as well as by some ATL cells (Fig. 2B).

CD44 staining was observed in tumor cells of 6 of the 7 ATL patients and in macrophage cells in all but patient 2 (Table 3). But compared to OPN staining, CD44 staining was apparently more evident in ATL tumor cells (Fig. 2). For CD44v6 staining, tumor cells were only weakly positive in patients 5 and 6 (Table 3); as shown in Fig. 2A and B, the cells in epidermis were positive for CD44v6, but the tumor cells and macrophage cells in NALT were negative.

Table 4
FACS analysis showed integrin α4 is positive in 43T and ED40515.

Antibody	Clone	43T	ED40515
CD49d (integrin α4)	9F10	99%	95%
CD29 (integrin β1)	TS2/16	N	N
Integrin β7	FIB504	N	N
CD44	F10-44-2	N	N
CD44v6	VFF-7	N	N
CD25	2A3	99%	95%
HLA-DR	G46-6	97%	91%

Abbreviation: N, negative.

3.4. The expression of integrin and CD44 in the ATL cell lines

Further, to investigate the interaction and relationship between OPN and its receptor integrin and CD44, we utilized 43-T and ED40515 cells ATL cell lines in vitro. First, we examined the OPN production of 43-T and ED40515 cells and found that the ATL cell line itself produces lower amounts of OPN in vitro compared with the macrophage cell line of A-THP-1 cells. The levels of OPN in the supernatants in the 43-T, ED40515 and A-THP-1 cell lines were 200 pg/ml, 400 pg/ml and 43 ng/ml, respectively. Then, we measured the expressions of integrin α4, β1, β7, and CD44 and CD44v6 with CD25 and HLA-DR as the positive controls in 43-T and ED40515 cells. FACS analysis showed that both cell lines were positive for α4 integrin, CD25 and HLA-DR, but negative for integrin β1, β7 and CD44, CD44v6 (Table 4).

Therefore, we could not detect interaction between OPN and CD44 or CD44v6 in the above ATL cell lines, but could show that the α4 integrin expression of 43-T was inhibited by both rOPN and the supernatant OPN from A-THP-1, whereas those of CD25 and HLA-DR were not inhibited (Fig. 3A and C).

4. Discussion

In this study, the clinicopathological roles of both OPN and sCD44 in ATL were studied. Our results showed that the plasma levels of both molecules were elevated in ATL patients and the levels were significantly different among normal and the four ATL subtypes. Furthermore, the two molecules were significantly correlated and both levels were clinically associated with the prognostic factors of ATL of PS, TIL, LDH and Ly. However, the level of OPN had strong correlations with clinical markers such as PS and TIL, whereas that of sCD44 was correlated with laboratory markers such as Ly and LDH. The correlation of OPN with TIL was explained in part by its chemoattractive activity [35], but these distinctly different correlations between OPN and sCD44 have not been described in other human cancers. In acute myeloid leukemia, OPN was proposed as potential prognostic and therapeutic target because related Ser585/PI3-kinase signaling pathway was deregulated [36]. Previously, it was reported that the expression of CD44 in Non-Hodgkin's lymphoma has a correlation with unfavorable clinical

Table 3
Immunohistochemical findings of OPN and CD44, CD44v6 staining in tissue of patients with ATL.

Patient no.	Age/sex	Diagnosis	Sample type	IHC findings			Plasma OPN (ng/ml)
				OPN-CSA II	CD44	CD44v6	
1	39F	ATL	Lymph-node	T−, M++, E+	T+, M+	T−	970
2	54F	ATL	Skin	T+, Epi+	T+, Epi+	T−, Epi+	610
3	48M	ATL	Nasal Cavity	T+, M++	T+, M++	T−	3550
4	59F	ATL	Lymph-node	T+, M++, E+	T+, M++	T−, F+	NA
5	70F	ATL	Lymph-node	T+, M+	T+/−, M+	T+/−	NA
6	48M	ATL	Lymph-node	T+, M+	T−, M+, E+	T+/−	NA
7	36M	ATL	Lymph-node	T+/−, M+, E+	T+, M+	T−	NA

Abbreviations: F, female; M, male; ATL, adult T cell Lymphoma; T, tumor cell; M, macrophage; E, endothelial cell; Epi, epithelial cell; NA, not available; −, negative; +/−, weakly positive; +, moderately positive; ++, strongly positive.

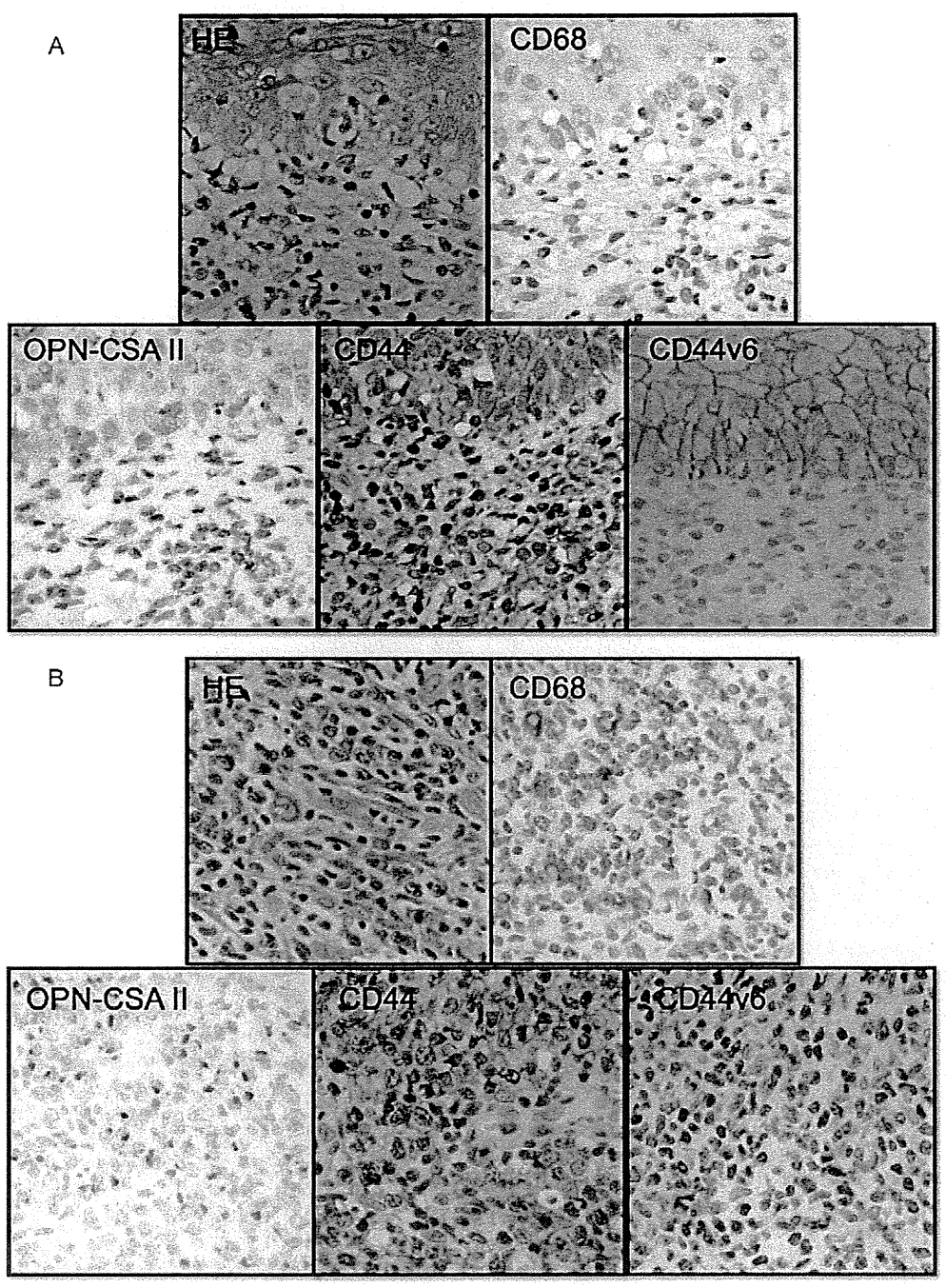

Fig. 2. Immunohistochemical stainings of CD68, OPN-CSA II, CD44 and CD44v6 in ATL. (A) Skin (patient 2); (B) nasal cavity-associated lymphoid tissue (NALT) (patient 3). All pictures were ×40 magnifications. (A) Hematoxylin and eosin (HE) staining showed upper layer of normal epidermis cells and ATL tumor cells. Few infiltrating CD68 positive macrophages were found in tumor area. ATL tumor cells as well as normal epidermis cells were positive for both OPN and CD44. However, the cells in the epidermis but not the ATL cells were positive for CD44v6. (B) HE staining showed tumor cells with markedly deformed nuclei. CD68-positive infiltrating macrophages also expressed OPN. These macrophages as well as tumor cells expressed CD44. Tumor cells from the ATL lacked the expression of the CD44v6.

prognosis, and CD44 was expressed by both lymphoma and reactive cells [37,23].

We next examined the expression of CD44 and OPN in ATL tissues. The source of OPN has been believed to be tumor cells [38] and/or other cells such as macrophages [39]. In our studies, OPN was only detected after the amplification and ATL cells synthesized OPN and/or CD44 weakly. We previously reported that Tax enhanced the expression of OPN and CD44 [25,26], however, it is also known that leukemic cells lack the expression of virus-related genes including Tax in ATL cells. The correlation of the expression of these molecules with that of Tax should be carefully examined in future *in vivo*. In normal lymph nodes, OPN staining was positive in B cells of Germinal Center (GC), endothelial cells and macrophages (data not shown). In the 6 ATL patients, infiltrated macrophage cells were positive for both OPN and CD44 and their intensities were much stronger than those of ATL tumor cells. Furthermore, we reported previously that cells from lymph nodes express more activated antigens such as CD38, Ki-67, CD7 and HLA-DR than peripheral blood leukemic cells in ATL, and proposed that ATL cells proliferate mainly in the lymph nodes [40].

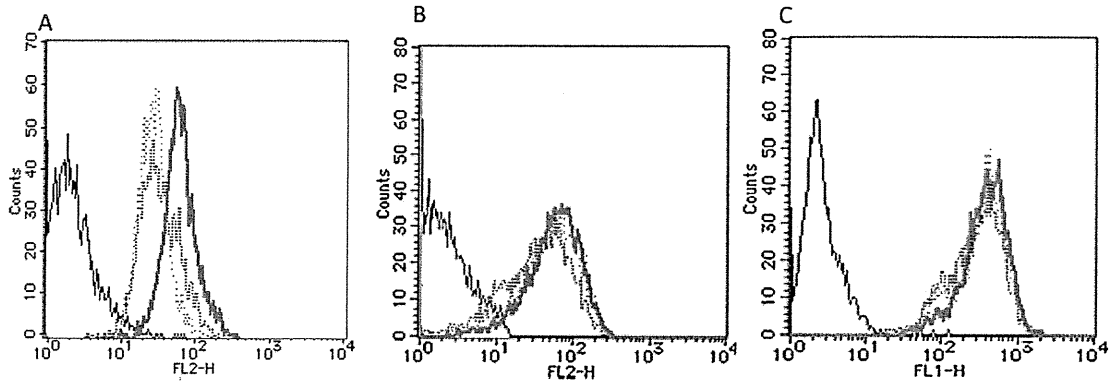

Fig. 3. Recombinant OPN (rOPN) inhibits the binding of antibody against integrin α4 but not those of CD25 and HLA-DR in 43-T cells. 43-T cells were cultured with FBS free RPMI for 24 h at 37 °C with 5% CO_2 and were treated 30 min with 3 μg/ml of rOPN or A-THP-1 supernatant at 4 °C followed by FACS analysis after washing. Both rOPN and A-THP-1 supernatant inhibited the binding of antibody against integrin α4 (A), but not that of CD25 (B) or HLA-DR (C). The color of each line: black, isotype; green, control; pink: rOPN; blue: A-THP-1 supernatant. (For interpretation of the references to color in this figure legend, the reader is referred to the web version of this article.)

Therefore, probably the increased plasma levels of OPN in ATL are derived from tumor-associated (infiltrated) macrophages and tumor cells in the enlarged lymph nodes of ATL. It is quite interesting that, macrophages cells in the involved lymph-nodes of the ATL were moderately or strongly positive for both OPN and CD44. Tumor-associated macrophages are known to be the M2 phenotype that promotes tumor proliferation [41]. Also, recent research revealed that increased numbers of CD68-positive tumor-associated macrophages in lymph nodes were strongly associated with treatment failure, relapse and shortened survival in patients of classic Hodgkin's lymphoma [42]. Although the signaling of OPN through CD44 was implicated to be important in breast cancers, and tumor-associated macrophages were reported to synthesize OPN and CD44 in an experimental mouse model [43], this is the first report that both molecules were found in macrophages and tumor cells in human diseases. Moreover, although a number of cytokines were known to be released from HTLV-1 infected cell lines or fresh tumor cells, none of them were found to be correlated with the prognosis [11–13]. However, CD44v6 expression in infiltrating ATL cells was found only in two cases and it was unexpectedly strongly expressed in the epidermis. In addition, ATL cell lines of 43-T and ED40515 were negative for both CD44 and CD44v6, but positive for integrin α4. Although, we could not detect integrin β1 and β7 on these cell lines, the presence of functional integrins were strongly suggested because 43-T cells responded chemotactic signals by OPN (unpublished observation). Further analysis of integrins on these cell lines is underway. Furthermore, abundant expression of OPN in epidermal cells was noted, which may be the cause of the frequent skin involvement in ATL because OPN is also known as a chemoatrractant agent [35]. Also, it would be of interest to determine if the cells of the epidermis in ATL patients synthesize more OPN than that of normal individuals.

Consequently, this is the first report describing both OPN and CD44 expression in ATL. Because OPN-CD44 axis was found to be associated with the prognosis of ATL patients, these molecules could be potential targets in this aggressive disease. However, since the numbers of patients studied here was small, it will be necessary to investigate the roles of OPN and CD44 in a larger number of patients. It would also be important to determine whether these molecules could be markers to detect the progression of the disease in HTLV-1 infected carriers.

Taken together, we clarified that elevated levels of plasma OPN and sCD44 were associated with the disease severity in ATL patients and that they were expressed in lymph-node and skin. Due to their multiple biological activities, both could be prognostic markers of ATL.

Author's contributions

H.C.-Y. performed the research and wrote the manuscript; K.T. supplied the plasma of ATL and their clinical data; Y.T. performed the immunohistochemical staining; S.O. did the statistic analysis; H.H. supplied tissue and clinical information of ATL patients; N.I. participated in FACS study; J.Z. participated discussion of the activities of Tax and OPN; M.F. analyzed the immunohistochemical staining; T.H. designed the study and edited the manuscript, and is responsible for all the work.

Conflict of interest

The authors declare no competing financial interest.

Acknowledgements

We would like to thank the ATL patients who participated in the study. We are grateful to Prof. T. Uede (Hokkaido University) for kind suggestions on our experiments and to Dr. M. Maeda (Kyoto University) for providing the 43-T and ED40515 cells. Also, we appreciate Dr. A. Kasajima (Tohoku University Hospital) for kind help in interpreting the slides of immunohistochemical staining.

This work was supported by collaborative funding from the Research Center for Zoonosis Control, Hokkaido University.

References

[1] Poiesz BJ, Ruscetti FW, Gazdar AF, et al. Detection and isolation of type C retrovirus particles from fresh and cultured lymphocytes of a patient with cutaneous T-cell lymphoma. Proc Natl Acad Sci USA 1980;77(12):7415.
[2] Hinuma Y, Nagata K, Hanaoka M, et al. Adult T-cell leukemia: antigen in an ATL cell line and detection of antibodies to the antigen in human sera. Proc Natl Acad Sci USA 1981;78(10):6476.
[3] Uchiyama T, Yodoi J, Sagawa K, Takatsuki K, Uchino H. Adult T-cell leukemia: clinical and hematologic features of 16 cases. Blood 1977;50:481.
[4] Shimoyama M. Diagnostic criteria and classification of clinical subtypes of adult T-cell leukaemia–lymphoma: a report from the Lymphoma Study Group (1984–1987). Br J Haematol 1991;79:428.
[5] Tsukasaki K, Hermine O, Bazarbachi A, et al. Definition, prognostic factors, treatment, and response criteria of adult T-cell leukemia–lymphoma: a proposal from an international consensus meeting. J Clin Oncol 2008;27:453.
[6] Hattori T, Uchiyama T, Toibana T, Takatsuki K, Uchino H. Surface phenotype of Japanese adult T-cell leukemia cells characterized by monoclonal antibodies. Blood 1981;58(3):645.
[7] Suzushima H, Asou N, Nishimura S, et al. Double-negative (CD4– CD8–) T cells from adult T-cell leukemia patients also have poor expression of the T-cell receptor alpha beta/CD3 complex. Blood 1993;81(4):1032.
[8] Kikuchi M, Mitsui T, Matsui N, et al. T-cell malignancies in adults: histopathological studies of lymph nodes in 110 patients. Jpn J Clin Oncol 1979;9:407.

[9] Arisawa K, Soda M, Endo S, et al. Evaluation of adult T-cell leukemia/lymphoma incidence and its impact on non-Hodgkin lymphoma incidence in southwestern Japan. Int J Cancer 2000;85(3):319.
[10] Grassmann R, Dengler C, Müller-Fleckenstein I, et al. Transformation to continuous growth of primary human T lymphocytes by human T-cell leukemia virus type I X-region genes transduced by a Herpes virus saimiri vector. Proc Natl Acad Sci USA 1989;86:3351.
[11] Wano Y, Hattori T, Matsuoka M, et al. Interleukin 1 gene expression in adult T-cell leukemia. J Clin Invest 1987;80:911.
[12] Chung HK, Young HA, Goon PK, et al. Activation of interleukin-13 expression in T cells from HTLV-I-infected individuals and in chronically infected cell lines. Blood 2003;102:4130.
[13] Chen J, Petrus M, Bryant BR, et al. Induction of the IL-9 gene by HTLV-I Tax stimulates the spontaneous proliferation of primary adult T-cell leukemia cells by a paracrine mechanism. Blood 2008;111(10):5163.
[14] Satou Y, Yasunaga J, Yoshida M, Matsuoka M. HTLV-I basic leucine zipper factor gene mRNA supports proliferation of adult T cell leukemia cells. Proc Natl Acad Sci USA 2006;103(3):720.
[15] Katagiri YU, Sleeman J, Fujii H, et al. CD44 variants but not CD44 s cooperate with beta1-containing integrins to permit cells to bind to osteopontin independently of arginine–glycine–aspartic acid, thereby stimulating cell motility and chemotaxis. Cancer Res 1999;59(1):219.
[16] Green PM, Ludbrook SB, Miller DD, Horgan CM, Barry ST. Structural elements of the osteopontin SVVYGLR motif important for the interaction with alpha(4) integrins. FEBS Lett 2001;503(1):75.
[17] Bellahcène A, Castronovo V, Ogbureke KU, Fisher LW, Fedarko NS. Small integrin-binding ligand N-linked glycoproteins (SIBLINGs): multifunctional proteins in cancer. Nat Rev Cancer 2008;8(3):212.
[18] Chagan-Yasutan H, Saitoh H, Ashino Y, et al. Persistent elevation of plasma osteopontin levels in HIV patients despite highly active antiretroviral therapy. Tohoku J Exp Med 2009;218:285.
[19] McAllister SS, Gifford AM, Greiner AL, et al. Systemic endocrine instigation of indolent tumor growth requires osteopontin. Cell 2008;133(6):994.
[20] Aruffo A, Stamenkovic I, Melnick M, Underhill CB, Seed B. CD44 is the principal cell surface receptor for hyaluronate. Cell 1990;61(7):1303.
[21] Weber GF, Ashkar S, Glimcher MJ, Cantor H. Receptor–ligand interaction between CD44 and osteopontin (Eta-1). Science 1996;271(5248):509.
[22] Ponta H, Sherman L, Herrlich PA. CD44: from adhesion molecules to signalling regulators. Nat Rev Mol Cell Biol 2003;4(1):33.
[23] Stauder R, Eisterer W, Thaler J, Günthert U. CD44 variant isoforms in non-Hodgkin's lymphoma: a new independent prognostic factor. Blood 1995;85(10):2885.
[24] Wielenga VJ, van der Neut R, Offerhaus GJ, Pals ST. CD44 glycoproteins in colorectal cancer: expression, function, and prognostic value. Adv Cancer Res 2000;77:169.
[25] Zhang J, Yamada O, Matsushita Y, Chagan-Yasutan H, Hattori T. Transactivation of human osteopontin promoter by human T-cell leukemia virus type 1-encoded Tax protein. Leuk Res 2009;34:763.
[26] Zhang J, Yamada O, Kida S, Matsushita Y, Yamaoka S, et al. Identification of CD44 as a downstream target of noncanonical NF-kB pathway activated by Human T-cell leukemia virus type 1-encoded Tax protein. Virology 2011;413:244.
[27] Chagan-Yasutan H, Shiratori B, Siddiqi UR, et al. The increase of plasma galectin-9 in a patient with insulin allergy: a case report. Clin Mol Allergy 2010;8(1):12.
[28] Chen R, Sigdel TK, Li L, et al. Differentially expressed RNA from Public microarray data identifies serum protein biomarkers for cross-organ transplant rejection and other conditions. PLoS Comput Biol 2010;6(9):e1000940.
[29] Shibata H, Yamakoshi H, Sato A, et al. Newly synthesized curcumin analog has improved potential to prevent colorectal carcinogenesis in vivo. Cancer Sci 2009;100(5):956.
[30] Gao C, Guo H, Downey L, et al. Osteopontin-dependent CD44v6 expression and cell adhesion in HepG2 cells. Carcinogenesis 2003;24(12):1871.
[31] Takemoto M, Yokote K, Nishimura M, et al. Enhanced expression of osteopontin in human diabetic artery and analysis of its functional role in accelerated atherogenesis. Arterioscler Thromb Vasc Biol 2000;20(3):624.
[32] Hattori T, Asou N, Suzushima H, et al. Leukaemia of novel gastrointestinal T-lymphocyte population infected with HTLV-I. Lancet 1991;337(8733):76.
[33] Tominaga T, Suzuki M, Saeki H, et al. Establishment of an activated macrophage cell line. A-THP-1, and its properties. Tohoku J Exp Med 1998;186(2):99.
[34] Major prognostic factors of patients with adult T-cell leukemia-lymphoma: a cooperative study—Lymphoma Study Group (1984–1987). Leuk Res 1991;15:81.
[35] Weiss JM, Renkl AC, Maier CS, et al. Osteopontin is involved in the initiation of cutaneous contact hypersensitivity by inducing Langerhans and dendritic cell migration to lymph nodes. J Exp Med 2001;194(9):1219.
[36] Powell JA, Thomas D, Barry EF, et al. Expression profiling of a hemopoietic cell survival transcriptome implicates osteopontin as a functional prognostic factor in AML. Blood 2009;114(23):4859.
[37] Horst E, Meijer CJ, Radaszkiewicz T, et al. Adhesion molecules in the prognosis of diffuse large-cell lymphoma: expression of a lymphocyte homing receptor (CD44), LFA-1 (CD11a/18), and ICAM-1 (CD54). Leukemia 1990;4(8):595.
[38] Castellano G, Malaponte G, Mazzarino MC, et al. Activation of the osteopontin/matrix metalloproteinase-9 pathway correlates with prostate cancer progression. Clin Cancer Res 2008;14(22):7470.
[39] Hsu HP, Shan YS, Lai MD, Lin PW. Osteopontin-positive infiltrating tumor-associated macrophages in bulky ampullary cancer predict survival. Cancer Biol Ther 2010;10(2):144.
[40] Shirono K, Hattori T, Hata H, Nishimura H, Takatsuki K. Profiles of expression of activated cell antigen on peripheral blood and lymph node cells from different clinical stages of adult T-cell leukemia. Blood 1989;73:1664.
[41] Solinas G, Germano G, Mantovani A, Allavena P. Tumor-associated macrophages (TAM) as major players of the cancer-related inflammation. J Leukocyte Biol 2009;86(5):1065.
[42] Steidl C, Lee T, Shah SP, et al. Tumor-associated macrophages and survival in classic Hodgkin's lymphoma. N Engl J Med 2010;362(10):875.
[43] Duff MD, Mestre J, Maddali S, et al. Analysis of gene expression in the tumor-associated macrophage. J Surg Res 2007;142(1):119.

Journal of
Synchrotron
Radiation

ISSN 0909-0495

Received 26 October 2010
Accepted 30 March 2011

A narrow microbeam is more effective for tumor growth suppression than a wide microbeam: an *in vivo* study using implanted human glioma cells

Atsushi Uyama,[a]* Takeshi Kondoh,[a] Nobuteru Nariyama,[b] Keiji Umetani,[b] Manabu Fukumoto,[c] Kunio Shinohara[d] and Eiji Kohmura[a]

[a]Department of Neurosurgery, Kobe University Graduate School of Medicine, Kobe, Hyogo 650-0017, Japan, [b]Japan Synchrotron Radiation Research Institute, Hyogo, Japan, [c]Institute of Development, Aging and Cancer, Tohoku University, Sendai, Japan, and [d]Advanced Research Institute for Science and Engineering, Waseda University, Tokyo, Japan.
E-mail: auyama811@yahoo.co.jp

The tumoricidal mechanisms of microbeam radiation therapy, and the more recently proposed minibeam radiation therapy, for the treatment of brain tumors are as yet unclear. Moreover, from among the various parameters of beam geometry the impact of changing the beam width is unknown. In this study, suppression of tumor growth in human glioma cells implanted in mice was evaluated experimentally using microbeams of two different widths: a conventional narrow beam (20 μm width, 100 μm center-to-center distance) and a wide beam (100 μm width, 500 μm center-to-center distance). The tumor growth ratio was compared and acute cell death was studied histologically. With cross-planar irradiation, tumor growth was significantly suppressed between days 4 and 28 after 20 μm microbeam irradiation, whereas tumor growth was suppressed, and not significantly so, only between days 4 and 18 after 100 μm microbeam irradiation. Immunohistochemistry using TUNEL staining showed no increase in TUNEL-positive cells with either microbeam at 24 and 72 h post-irradiation. The 20 μm microbeam was found to be more tumoricidal than the 100 μm microbeam, and the effect was not related to apoptotic cell death. The underlying mechanism may be functional tissue deterioration rather than direct cellular damage in the beam path.

Keywords: microbeam radiation therapy; narrow microbeam; wide microbeam; co-planar microbeam; cross-planar microbeam.

1. Introduction

Microbeam radiation therapy (MRT), which was originally introduced for the treatment of brain tumors by Slatkin *et al.* (1992), uses a parallel array of microbeams, the so-called 'co-planar microbeam', composed of high-intensity and highly directional X-rays generated at a synchrotron radiation facility. The principle of this treatment is based on the high resistance of normal brain tissue to such irradiation. This phenomenon was first observed in experiments concerning the biological effects of cosmic rays in the late 1950s. Zeman *et al.* (1961) reported that a microscopic (25 μm) 22 MeV deuteron beam required a dose of over 4000 Gy to kill cells in the beam path in the mouse cortex, compared with a macroscopic (1 mm) beam of only 140 Gy which destroyed all tissue in its path.

Recently, Bräuer-Krisch *et al.* (2010) comprehensively reviewed the several *in vivo* studies of MRT that have been carried out in rodents. These studies used various tumor cell lines: glioma (Schültke *et al.*, 2008), gliosarcoma (Laissue *et al.*, 1998; Dilmanian *et al.*, 2002; Smilowitz *et al.*, 2006; Regnard *et al.*, 2008; Serduc *et al.*, 2008, 2009*a*,*b*), squamous cell carcinoma (Miura *et al.*, 2006) and mammary tumor (Dilmanian *et al.*, 2003) cell lines. The implantation site was either brain parenchyma or the flanks near the hind legs. The results of these studies provided clear evidence that MRT was associated with the suppression of tumor growth (Dilmanian *et al.*, 2003; Miura *et al.*, 2006) and the extension of life of the rodents implanted with tumors (Laissue *et al.*, 1998; Dilmanian *et al.*, 2002; Smilowitz *et al.*, 2006, 2008, 2009*a*,*b*; Regnard *et al.*, 2008; Schültke *et al.*, 2008).

In MRT, the geometry of the microbeam is defined by the parameters of beam width, center-to-center distance, peak dose and valley dose (Fig. 1). In previous reports these parameters were in the range 25–90 μm, 50–300 μm, 150–900 Gy and 12.1–40 Gy, respectively (Laissue *et al.*, 1998; Dilmanian *et*

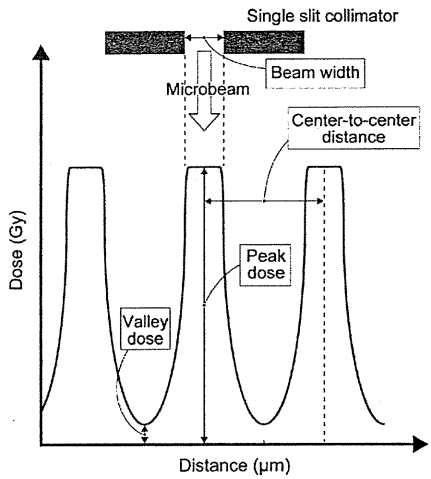

Figure 1
Schematic geometry of microbeam arrays used in MRT.

al., 2002, 2003; Miura *et al.*, 2006; Smilowitz *et al.*, 2006; Schültke *et al.*, 2008; Regnard *et al.*, 2008; Serduc *et al.*, 2008, 2009*a*,*b*). Most of these MRT studies used a narrow beam with a width of around 30 μm. However, such a narrow beam can be generated only by a large-scale synchrotron radiation facility. Since the number of such facilities is limited, a more practical beam for clinical purposes, the so-called 'minibeam' or 'thick microbeam', has recently been introduced for radiation therapy (Dilmanian *et al.*, 2006, 2008; Anschel *et al.*, 2007; Prezado *et al.*, 2009). A parallel array of thick beams (500–700 μm) is used to produce such a beam. However, the tumoricidal effects obtained with different beam widths have not yet been compared. It should also be emphasized that previous studies have needed a high valley dose (12.1–40 Gy), which might result in unacceptable irradiation levels in the valley area. Indeed, Bräuer-Krisch *et al.* (2010) state that the valley dose is the most important determinant of normal tissue damage in MRT.

The purpose of this study was to compare tumor growth in human U251 glioma cells following microbeam radiation treatment using microbeams of two different widths (20 μm and 100 μm). For this purpose an adjustable collimator, which enables modulation of the variable peak width, was used for the first time. To avoid any tumoricidal effect caused by valley irradiation, we chose a relatively low dose of irradiation, with the valley dose set as low as 4.8–9.6 Gy. We then assessed the effect of MRT by measuring the volume of tumors irradiated over time and recording the histological findings of tumors in the acute phase after irradiation.

2. Materials and methods

2.1. Experimental groups

Thirty-six mice implanted with tumors were divided into a MRT-treated group (n = 28) and a control group (n = 8). The MRT-treated group was then further divided into four subgroups: (i) a co-planar MRT group where microbeams 100 μm wide with a 500 μm center-to-center distance were used ('co-planar 100'; n = 8); (ii) a cross-planar MRT group where microbeams 100 μm wide with a 500 μm center-to-center distance were used ('cross-planar 100'; n = 8); (iii) a cross-planar MRT group where microbeams 20 μm wide with a 100 μm center-to-center distance were used ('cross-planar 20'; n = 6); and (iv) a repeated cross-planar MRT group where microbeams 100 μm wide with a 500 μm center-to-center distance were delivered once a day for two days ('cross-planar 100 × 2'; n = 6).

2.2. Preparation of tumor model

All procedures involving animals were approved by the Animal Care and Use Review Committee of Kobe University Graduate School of Medicine. Male five-week-old nude mice (BALB/cAJc1-nu/nu) weighing 20–25 g (Clea Japan, Osaka, Japan) were housed in an approved specific pathogen-free facility at Kobe University in accordance with Laboratory Animal Resources Commission standards. Appropriate care was taken to minimize animal discomfort, and appropriate sterile surgical techniques were utilized for tumor implantation and drug administration. U251 human glioma cells were maintained in Dullbecco's modified Eagle's medium containing glutamine, 10% fetal bovine serum, penicillin/streptomycin, and grown at 310 K in a 5% CO2 incubator. Ten days before MRT, the tumor cells were concentrated to 6 × 10^6 per 200 μl and implanted subcutaneously into the flanks near the hind legs of mice anesthetized with halothane inhalation.

2.3. Radiation source

MRT was performed at SPring-8, a large-scale synchrotron radiation facility in Japan. The radiation source was generated at the white X-ray bending-magnet beamline BL28B2. The radiation beam traveled in a vacuum transport tube with minimized air scattering of the primary beam. X-rays passed from the vacuum tube into the atmosphere through a beryllium vacuum window, then into a 2.0 m helium beam path consisting of an aluminium tube and a thin aluminium helium window located 42 m from the synchrotron radiation output. The sample positioning system was placed 2.5 m from the thin aluminium window. A 3 mm-thick copper filter was inserted into the beam to remove the low-energy component. The X-ray spectrum was in the range 50–200 keV, peaking at around 90 keV. The air kerma rate of the broad beam was measured with a free-air ionization chamber. The electrode gap was 85 mm, which kept the electron escape fraction from the chamber below 3%, at 50–200 keV (Nariyama *et al.*, 2004). Near current saturation was obtained by applying a voltage of 9.5 kV.

2.4. Collimator and irradiation

MRT was performed with the aid of an adjustable single-slit collimator which enabled a variable spatial fractionation of the X-ray beam (Fig. 2*a*). The microbeam width was equal to the distance between two plates of tantalum. The center-to-

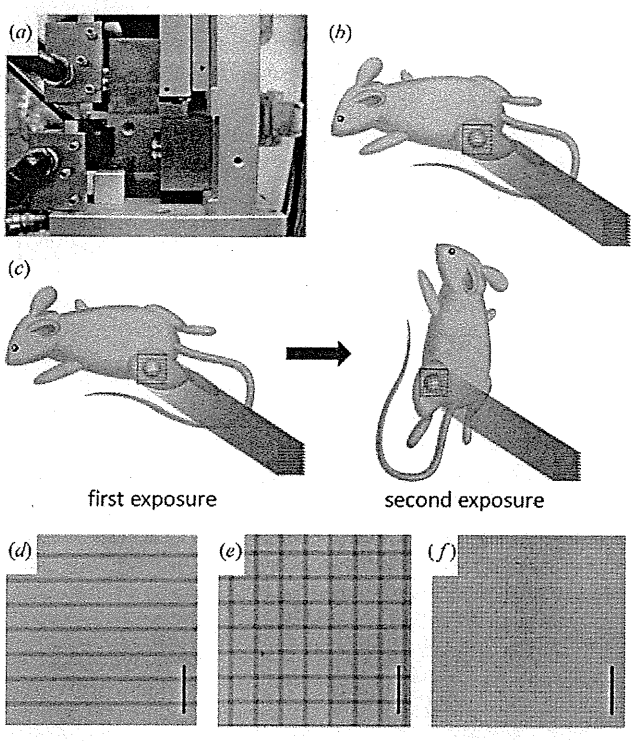

Figure 2
(*a*) An adjustable single-slit collimator which enables modulation of the variable peak width. (*b*) For co-planar microbeam irradiation, mice were treated with a single set of irradiation in the prone position. (*c*) For cross-planar microbeam irradiation, mice were irradiated in stages by means of 90° rotation about the axis parallel to the microbeams. (*d–f*) The spatial dose distribution was confirmed using GafChromic film for 'co-planar 100' (*d*), 'cross-planar 100' (*e*) and 'cross-planar 20' (*f*). Scale bar: 1 mm.

center distance between one beam and the next beam was determined by horizontally moving the platform holding the experimental animal. An anesthetized mouse (sodium pentobarbital; 0.5 mg per 10 g of body weight, i.p.) was placed on the platform in the prone position lying on a styrol box. The hind leg with the tumor was immobilized with a plastic ring in a direction perpendicular to the microbeams. For the 'co-planar MRT' irradiation, mice received a single irradiation treatment in the prone position (Fig. 2*b*); for the 'cross-planar MRT', mice received staged irradiation, first receiving irradiation as performed for 'co-planar MRT', followed by a second irradiation in the vertical position by rotating the axis by 90° so that the head was up (Fig. 2*c*). The radiation field was 15 mm wide and 15 mm high.

The spatial dose distribution was examined using GafChromic film HD-810 (ISP Technologies, NJ, USA) as described previously (Nariyama *et al.*, 2009) (Figs. 2*d*–2*f*). The optical density of the irradiated films was measured with a digital microscope through bandpass filters, and converted to dose using a calibration curve obtained in advance. The bandpass filters of 601 and 668 nm were used to attain the straight line for the calibration curve and increase the sensitivity and accuracy; the former was used for the peak dose and the latter for the valley dose.

2.5. Dose rate setting

The air kerma rate was preset at 140 Gy s^{-1} at the hutch. With the newly designed adjustable collimeter the X-ray peak dose rates were found to be 124 Gy s^{-1} and 111 Gy s^{-1} for the 100 μm and 20 μm microbeams, respectively (Figs. 3*a* and 3*b*). The dose rate at a distance of 250 μm from the center of the 100 μm microbeam was 4.8 Gy s^{-1} (Fig. 3*a*), while that at a distance of 50 μm from the center of the 20 μm microbeam was 4.1 Gy s^{-1} (Fig. 3*b*). The duration of irradiation was 1 s, in order to keep the valley dose low while ensuring sufficient cell damage at peak dose. The valley dose of the cross-planar microbeam was double that of the co-planar microbeam at the same peak dose. For 'co-planar 100', 'cross-planar 100' and 'cross-planar 20', the cumulative valley dose was 4.8 Gy, 9.6 Gy and 8.2 Gy, respectively.

2.6. Evaluation of tumor growth

Tumor volume was measured for the two perpendicular diameters (X, Y) and thickness (Z) two to three times per week for one month after irradiation, by a technical assistant who was not informed of the treatment protocol. Tumor volume (V) was estimated using the formula $V = X \times Y \times Z \times 0.52$ as described previously (Shichiri *et al.*, 2009). The relative growth ratio was defined as V(at individual measurement point)/V(at irradiation) and analyzed statistically.

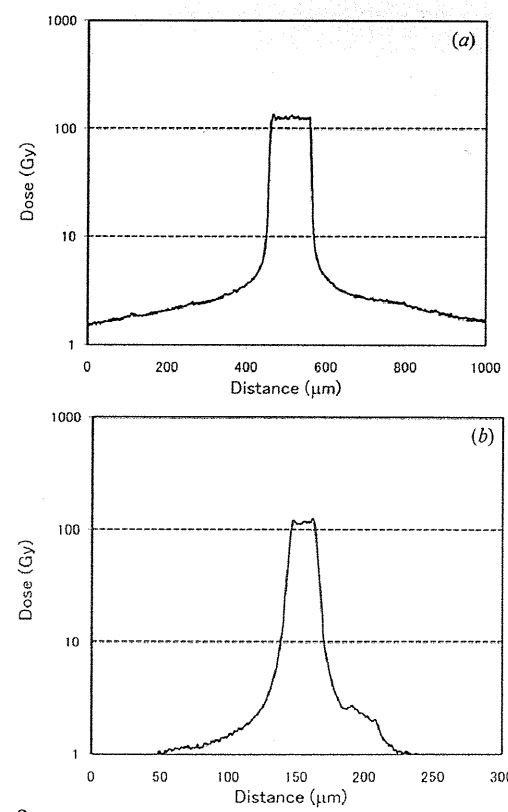

Figure 3
The spatial dose distribution was measured using GafChromic film in a 100 μm-wide microbeam (*a*) and 20 μm-wide microbeam (*b*). The peak dose was 130 Gy for both.

2.7. Histopathology

Forty-two mice were used for histopathological analysis. To determine the response to MRT, mice from the 'co-planar 100', 'cross-planar 100' and 'cross-planar 20' groups (excluding the 'cross-planar 100 × 2' group) were sacrificed at 24 and 72 h after irradiation (for all groups $n = 3$ for each time point). Three tumor-bearing mice that did not receive irradiation were sacrificed as controls at each of the same time points. To examine rapid pathological changes in the early post-irradiation phase, additional mice in the 'cross-planar 100' and 'cross-planar 20' groups were sacrificed at 3, 6 and 12 h after irradiation ($n = 3$ for each time point). After the mice had been deeply anesthetized, tumors were removed and fixed with 4% paraformaldehyde in phosphate-buffered saline (pH 7.4) for 24 h. Tumor tissue was cut along the horizontal plane perpendicular to the microbeams, embedded in paraffin, processed to yield 4 µm-thick sections, and stained with hematoxylin and eosin (HE).

Sections from the 'cross-planar 100' and 'cross-planar 20' groups obtained 24 and 72 h after irradiation as well as sections from the control mice were also used for detecting apoptosis by using the terminal deoxynucleotidyl transferase-mediated dUTP nick-end labeling (TUNEL) technique. The TUNEL reaction was performed with the ApoMark DNA Fragmentation Apoptosis Detection Kit (Exalpha Biologicals, Shirley, MA, USA) according to the manufacturer's instructions. The rate of apoptosis, calculated as the percentage of TUNEL-positive cells out of 1000 cells, was determined for 12 random tumor sections taken from three different tumors in each group.

2.8. Statistics

A one-way ANOVA was used to examine within-group differences in the tumor growth ratio at the individual time points post-irradiation and the difference in percentage of TUNEL-positive cells. For comparison between the groups, an additional *post-hoc* test was performed using the Turkey–Kramer method. The threshold for statistical significance was set at $p < 0.05$. Values are expressed in the figures as mean ± standard deviation (SD).

3. Results

3.1. Tumor growth

At irradiation the mean tumor volume (mm^3) for the control, 'co-planar 100', 'cross-planar 100', 'cross-planar 20' and 'cross-planar 100 × 2' groups were 43.8 ± 17.1, 37.1 ± 14.5, 34.8 ± 10.6, 34.7 ± 7.1 and 40.6 ± 13.3 (mean ± SD), respectively. As shown in Fig. 4, the groups showed suppression from lowest to highest in the order of 'co-planar 100', 'cross-planar 100', 'cross-planar 20' and 'cross-planar 100 × 2'. At 28 days after irradiation, tumor growth ratios of the control, 'co-planar 100', 'cross-planar 100', 'cross-planar 20' and 'cross-planar 100 × 2' groups reached 71.5 ± 68.7, 32.2 ± 19.6, 22.0 ± 16.2, 9.9 ± 7.9 and 9.6 ± 5.2, respectively (Fig. 4). When compared with the control group, the 'co-planar 100' group showed significant suppression of tumor growth ($p < 0.05$) at 4, 7 and 10 days post-irradiation, the 'cross-planar 100' group showed significant suppression at 4, 7, 10, 14 and 18 days post-irradiation, and the 'cross-planar 20' and 'cross-planar 100 × 2' showed significant suppression at 4, 7, 10, 14, 18, 21, 25 and 28 days post-irradiation. Thus, the 'cross-planar 20' group showed longer tumor growth suppression than the 'cross-planar 100' group, and the 'cross-planar 100 × 2' group showed suppression comparable with that of the 'cross-planar 20' group.

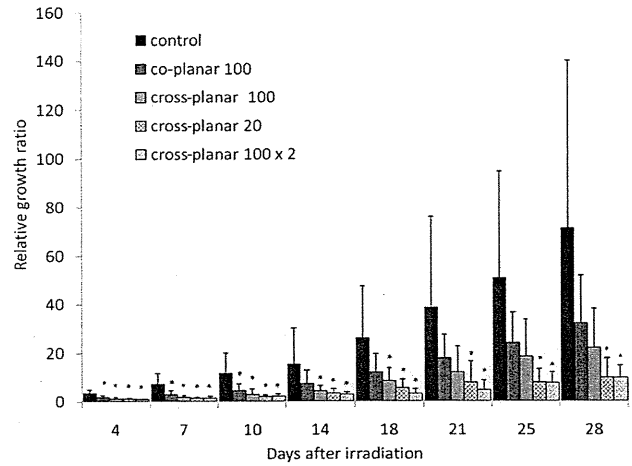

Figure 4
The relative growth ratios at various measurement time points during a 28 day period compared with measurements obtained at irradiation for 'control', 'co-planar 100', 'cross-planar 100', 'cross-planar 20' and 'cross-planar 100 × 2'. The asterisks indicate $p < 0.05$ when compared with the control group at a given time point.

3.2. Histological study

HE-stained sections of the non-irradiated control mice showed a large and dense cellular mass with marked pleomorphism. Endothelial hypertrophy was not evident, a few necrotic regions were located in the center of mass, and typical palisading cells were seen around the necrotic lesion (Fig. 5*a*). Irradiated HE-stained sections showed dark stripes along the beam path at low magnification at 24 h post-irradiation. The path was clearly seen in the 'co-planar 100', 'cross-planar 100' and 'cross-planar 20' groups (Figs. 5*b*, 5*c*, 5*e*), and a dense closely compacted cellular arrangement was observed on the path (Figs. 5*d*, 5*f*). The nuclei were more darkly stained than the nuclei of non-irradiated tumors. There were no microhemorrhages or non-viable cells in the area between the peaks. The path itself in the 'cross-planar 20' group was narrow and faint, and the area between the peaks showed intercellular edema. The size of the necrotic lesion differed in each of the treated tumors but no small cavitations that would indicate new pathological developments were seen (Figs. 5*d*, 5*f*). The dark stripes along the beam path remained at 72 h post-irradiation (Figs. 5*g*, 5*h*). A comparison of the rapid pathological changes in the early post-irradiation phase in the 'cross-planar 100' and 'cross-planar 20' groups revealed darkly

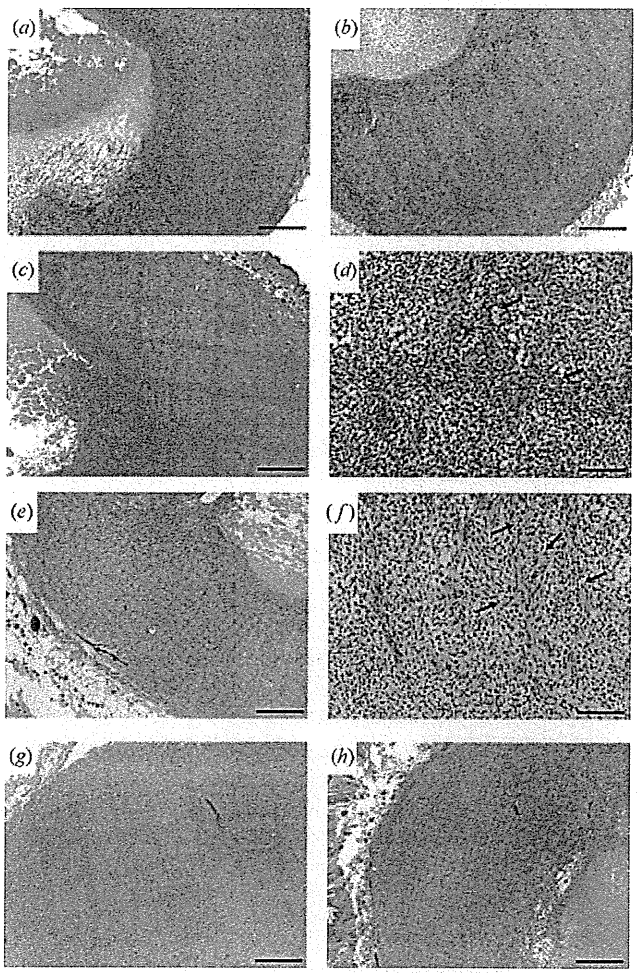

Figure 5
HE-stained sections of control (*a*), and 24 h after irradiation with 'co-planar 100' (*b*), 'cross-planar 100' (*c–d*) and 'cross-planar 20' (*e–f*), showing dark stripes along the beam path. The dark stripes remained 72 h after irradiation with 'cross-planar 100' (*g*) and 'cross-planar 20' (*h*). Arrows: microbeam path. Scale bar for (*a*), (*b*), (*c*), (*e*), (*g*), (*h*): 500 µm; for (*d*), (*f*): 100 µm.

stained nuclei on the beam path in both groups at 6 h post-irradiation (Fig. 6).

TUNEL results showed few apoptotic regions in all of the irradiated fields (Fig. 7). The average percentage of TUNEL-positive cells was 0.56 ± 0.23 in the control group and 0.54 ± 0.11 in the 'cross-planar 100' group at 24 h post-irradiation, 0.53 ± 0.17 in the 'cross-planar 100' group at 72 h, 0.84 ± 0.37 in the 'cross-planar 20' group at 24 h, and 0.80 ± 0.42 in the 'cross-planar 100' group at 72 h (Fig. 8). The percentage was not significantly different between any two groups.

4. Discussion

We studied the effects of MRT with a greater beam width and center-to-center distance than reported previously in an animal model implanted with U251 human glioma cells. We demonstrated that microbeams with a greater beam width and

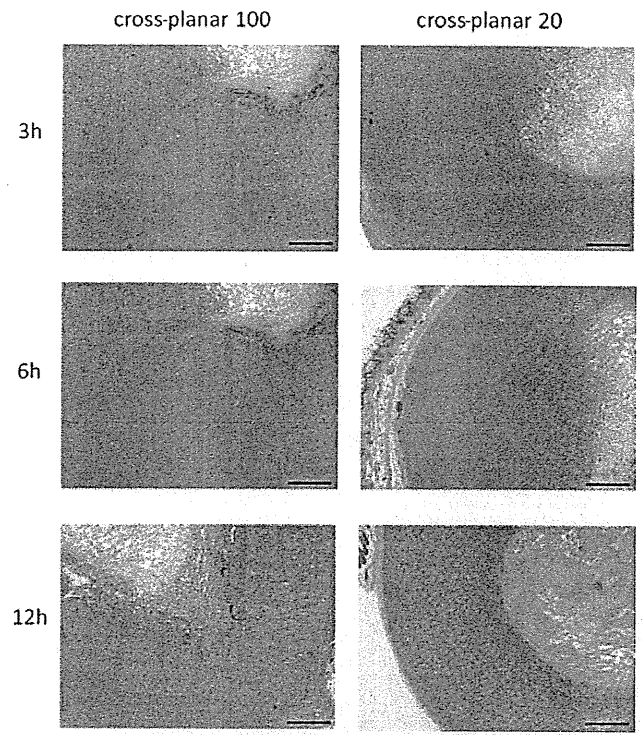

Figure 6
HE-stained sections 3, 6 and 12 h after irradiation with 'cross-planar 100' and 'cross-planar 20'. Scale bar: 500 µm.

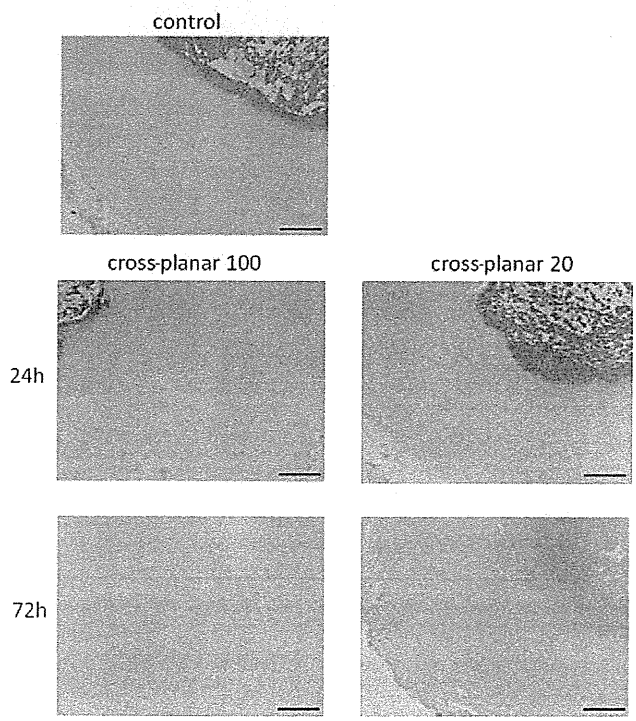

Figure 7
TUNEL staining of the sections irradiated with 'cross-planar 100' and 'cross-planar 20' showing few apoptotic regions in any of the irradiated fields at low magnification. Scale bar: 500 µm.

Table 1
Summary of previously reported experiments of MRT with animals.

Author; journal; year	Tumor cell line	Implantation site	Irradiation geometry	Beam width (μm)	Center-to-center distance (μm)	Peak dose (Gy)	Valley dose (Gy)	Evaluation criteria
Laissue *et al.*; *Int. J. Cancer*; 1998	9L gliosarcoma	Brain	Co-planar	25	100	625		Survival rate
			Orthogonal	25	100	312.5		Tumor size
			Orthogonal	25	100	625		Normal brain damage
Dilmanian *et al.*; *Neuro-Oncology*; 2002	9L gliosarcoma	Brain	Co-planar	27	50	150–300	20–40	Survival rate
			Co-planar	27	75	250–500	17–33	MRI (tumor size,
			Co-planar	27	100	500	19	normal brain damage)
Dilmanian *et al.*; *Radiat. Res.*; 2003	Murine EMT-6 mammary carcinoma	Hind leg	Co-planar	90	300	800–1900	16–38	Tumor size
			Cross-planar	90	300	410–650	16–26	Normal tissue toxicity
Smilowitz *et al.*; *J. Neuro-oncology*; 2006	9L gliosarcoma	Brain	Co-planar	25	211	625		Survival rate
Miura *et al.*; *Br. J. Radiol.*; 2006	Human squamaous cell carcinoma	Hind leg	Orthogonal	35	200	442		Tumor size
			Orthogonal	35	200	625		Normal tissue toxicity
			Orthogonal	35	200	884		
			Orthogonal	70	200	442		
Regnard *et al.*; *Phys. Med. Biol.*; 2008	9L gliosarcoma	Brain	Co-planar	25	100	625	36	Survival rate
			Co-planar	25	200	625	12.1	Clinical sign
								Body weight pattern
Serduc *et al.*; *Phys. Med. Biol.*; 2008	9L gliosarcoma	Brain	Orthogonal	25	211	500	24	Survival rate
								MRI (blood volume, vessel size)
Schültke; *Eur. J. Radiol.*; 2008	F98 glioma C6 glioma	Brain	Orthogonal	25	211	350		Survival rate
Serduc *et al.*; *Phys. Med. Biol.*; 2009	9L gliosarcoma	Brain	Orthogonal	25	211	860	36	Survival rate
			Orthogonal	50	211	480	36	
			Orthogonal	75	211	320	36	
Serduc *et al.*; *J. Synchrotron Rad.*; 2009	9L gliosarcoma	Brain	Three fractions through three orthogonal ports at 24 h intervals	50	211	400 (two directions) 360 (one direction)	15 per exposure	Survival rate Memory function
This work	Human U251 glioma	Hind leg	Co-planar	100	500	124	4.8	Tumor size
			Cross-planar	100	500	124	9.6	
			Cross-planar	20	100	111	8.2	

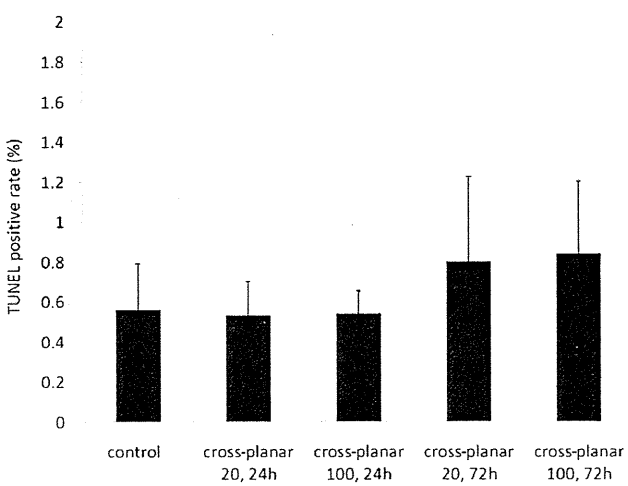

Figure 8
The percentages of TUNEL-positive cells are summarized.

center-to-center distance (100 μm and 500 μm, respectively) than reported previously (25–90 μm and 50–300 μm, respectively) produced moderate tumor growth suppression when applied in a cross-planar pattern, and that narrow microbeams with a width of 20 μm showed longer tumor growth suppression than microbeams with a width of 100 μm. These findings indicate that the tumor suppression effect of X-ray irradiation does not depend on the total amount of irradiated dose alone. Differences in spatial distribution also clearly affect tumor growth suppression and a narrow beam is more effective than a wide beam for MRT.

With regard to the mechanisms of tumor growth suppression, it could be suggested that the bystander effect of MRT affects tumor cells in the valley zone. However, our previous *in vitro* study using C6 glioma cells (Kashino *et al.*, 2009) demonstrated that such an effect is not sufficient to explain *in vivo* tumor growth suppression. At least, MRT-treated cells cultured in a dish do not exactly mimic the characteristics of MRT-treated cells *in vivo*.

Another possibility is that the tumoricidal effect of MRT results from the high biologically hazardous dosing of the valley zone, in other words, the background irradiation of all the targeted areas. To clarify this point we reviewed all previous MRT studies using animals reported in the literature (Table 1). Regardless of differences in tumor cell line, irradiation geometry, beam width, center-to-center distance or peak dose, we found that the valley doses used in these studies

were relatively high (12.1–40 Gy) and this has a direct effect on tumor cell growth in the valley zone. In particular, this dose could be critical when radiosensitive tumor cells are used. In previous studies of experimental radiosurgery on malignant brain tumors using a gamma knife unit the 50% marginal dose was 15–35 Gy, and cellular damage was histologically proven and survival rate significantly improved (Kondziolka *et al.*, 1992; Niranjan *et al.*, 2000, 2003; Nakahara *et al.*, 2001). To minimize the direct effect in the valley zone, our study used a lower dose (4.8–9.6 Gy) than used previously. Since a radiation dose < 10 Gy has never been reported to affect tumor cells *in vivo*, tumor growth suppression in the present study is unlikely to have resulted from the valley dose.

A double-strand break of DNA is fundamentally a direct acute cellular response to radiation and probably occurs in the peak area of both the wider (100 μm) and narrower (20 μm) microbeam. One unexpected result of the present study was that no significant change in the rate of apoptotic cells was detected by TUNEL staining. In another study it was found that a 35–70 Gy dose administered with a gamma knife unit did induce apoptotic cell death of 9L gliosarcoma between 6 and 48 h post-irradiation (Witham *et al.*, 2005) in a treated area 4 mm in diameter. However, in our study, microbeams of the order of 20 to 100 μm did not result in apoptotic tumor cell death even in the peak zone. No tissue death was induced either at the cellular or tissue level, because the necrotic area in each subgroup hardly changed after MRT. Therefore, the mechanism of tumor growth suppression in our study is likely to be the induction of lower cell proliferation.

Another possible mechanism of *in vivo* tumor suppression may be alteration of microvascular structures. Serduc *et al.* (2008) hypothesized that the tumoral vessel injury caused by MRT mainly affected tumor growth suppression, but they found no significant microvascular components, at least under their experimental conditions using 9L gliosarcoma implanted into the brain. We believe that further histological or functional studies of neovascularizing tumor vessels are required to identify the tumoricidal mechanism of MRT.

Recently, radiation therapy using a parallel array of thick beams (500–700 μm) with the same separation distance between beams, the so-called 'minibeam' or 'thick microbeam' therapy, has been recommended (Dilmanian *et al.*, 2006, 2008; Anschel *et al.*, 2007; Prezado *et al.*, 2009). Dilmanian *et al.* (2008) reported that this irradiation method at a peak dose of 170 Gy did not induce neurological deficits in rats. Although the biological mechanisms of the effects of such minibeams on tumor cells have not been thoroughly studied, our study demonstrated that the wide MRT of 'cross-planar 100' was as effective as the narrow MRT of 'cross-planar 20' when the wide MRT was applied once a day for two days. We therefore think that temporal fractionated MRT is useful for amplification of the tumoricidal effect of MRT.

Maintaining the proper balance between the tumoricidal and adverse effects of MRT on normal brain tissue and function is a challenging aspect in the refinement of the therapy. Regnard *et al.* (2008) reported on the effects of MRT by comparing the results obtained with 25 μm-wide co-planar beams with a 200 μm or 100 μm center-to-center distance. They found that MRT with a 200 μm center-to-center distance was superior in terms of sparing healthy tissue but that lifespan was longer with a 100 μm center-to-center distance. Schültke *et al.* (2008) reported that no memory dysfunction was detected in object recognition tests for rats treated with brain irradiation using 25 μm-wide microbeams with a 200 μm center-to-center distance and a skin entrance dose of 350 Gy. Whether wide MRT of 100 μm may affect normal brain tissue or function remains to be determined in future research.

In conclusion, MRT using a 100 μm-wide microbeam with 500 μm center-to-center distance resulted in moderate tumor growth suppression, although MRT using a 20 μm-wide microbeam resulted in longer tumor growth suppression. The biological mechanism underlying these findings is still unclear: it may involve functional tissue deterioration rather than direct cellular damage in the beam path. Further comparative experimental studies using both wide and narrow microbeams are warranted to determine the potential of MRT for clinical purposes.

We would like to thank Drs Koji Ono, Takashi Sasayama and Atsushi Arai for fruitful discussions, and Ayumi Katoh and Mariko Ueda for expert technical assistance. This study was supported in part by grants-in-aid for scientific research, (C)(2)(22591586) to TK from the Ministry of Education, Science, Sports and Culture of Japan. The synchrotron radiation experiments were performed at BL28B2 at SPring-8 with the approval of the Japan Synchrotron Radiation Research Institute (Proposals No. 2008B1627, 2009A1281 and 2009B1614).

References

Anschel, D. J., Romanelli, P., Benveniste, H., Foerster, B., Kalef-Ezra, J., Zhong, Z. & Dilmanian, F. A. (2007). *Minim. Invas. Neurosurg.* **50**, 43–46.

Bräuer-Krisch, E., Serduc, R., Siegbahn, E. A., Le Duc, G., Prezado, Y., Bravin, A., Blattmann, H. & Laissue, J. A. (2010). *Mutat. Res.* **704**, 160–166.

Dilmanian, F. A., Button, T. M., Le Duc, G., Zhong, N., Pena, L. A., Smith, J. A., Martinez, S. R., Bacarian, T., Tammam, J., Ren, B., Farmer, P. M., Kalef-Ezra, J., Micca, P. L., Nawrocky, M. M., Niederer, J. A., Recksiek, F. P., Fuchs, A. & Rosen, E. M. (2002). *Neuro-Oncology*, **4**, 26–38.

Dilmanian, F. A., Morris, G. M., Zhong, N., Bacarian, T., Hainfeld, J. F., Kalef-Ezra, J., Brewington, L. J., Tammam, J. & Rosen, E. M. (2003). *Radiat. Res.* **159**, 632–641.

Dilmanian, F. A., Romanelli, P., Zhong, Z., Wang, R., Wagshul, M. E., Kalef-Ezra, J., Maryanski, M. J., Rosen, E. M. & Anschel, D. J. (2008). *Eur. J. Radiol.* **68**, S129–S136.

Dilmanian, F. A., Zhong, Z., Bacarian, T., Benveniste, H., Romanelli, P., Wang, R., Welwart, J., Yuasa, T., Rosen, E. M. & Anschel, D. J. (2006). *Proc. Natl Acad. Sci. USA*, **103**, 9709–9714.

Kashino, G., Kondoh, T., Nariyama, N., Umetani, K., Ohigashi, T., Shinohara, K., Kurihara, A., Fukumoto, M., Tanaka, H., Maruhashi, A., Suzuki, M., Kinashi, Y., Liu, Y., Masunaga, S., Watanabe, M. & Ono, K. (2009). *Int. J. Radiat. Oncol. Biol. Phys.* **74**, 229–236.

Kondziolka, D., Lunsford, L. D., Claassen, D., Pandalai, S., Maitz, A. H. & Flickinger, J. C. (1992). *Neurosurgery*, **31**, 280–287.

Laissue, J. A., Geiser, G., Spanne, P. O., Dilmanian, F. A., Gebbers, J. O., Geiser, M., Wu, X. Y., Makar, M. S., Micca, P. L., Nawrocky,